AMERICAN UNIVERSITY OF BEIRUT

SPHINGOLIPIDOMICS OF ADENOVIRUS-INFECTED HUMAN LUNG ADENOCARCINOMA CELLS

by
HASAN MOHAMED HIJAZI

A thesis
submitted in partial fulfillment of the requirements
for the degree of Master of Science
to the Department of Biochemistry and Molecular Genetics
of the Faculty of Medicine
at the American University of Beirut

Beirut, Lebanon
March 2020

AMERICAN UNIVERSITY OF BEIRUT

SPHINGOLIPIDOMICS OF ADENOVIRUS-INFECTED HUMAN LUNG ADENOCARCINOMA CELLS

by

HASAN MOHAMED HIJAZI

Approved by:

Dr. Ghassan Dbaibo, MD — Advisor
Professor, Biochemistry and Molecular Genetics

Dr. Nadine Darwiche — Member of Committee
Professor, Biochemistry and Molecular Genetics

Dr. Firas Kobaissy — Member of Committee
Associate Professor, Biochemistry and Molecular Genetics

Dr. Hassan Zaraket — Member of Committee
Assistant Professor; Experimental Pathology, Immunology and Microbiology

Date of thesis/dissertation defense: [March 10, 2020]

AMERICAN UNIVERSITY OF BEIRUT

THESIS, DISSERTATION, PROJECT RELEASE FORM

Student Name: Hijazi Hasan Mohamed

◉ Master's Thesis ○ Master's Project ○ Doctoral Dissertation

☒ I authorize the American University of Beirut to: (a) reproduce hard or electronic copies of my thesis, dissertation, or project; (b) include such copies in the archives and digital repositories of the University; and (c) make freely available such copies to third parties for research or educational purposes.

☐ I authorize the American University of Beirut, to: (a) reproduce hard or electronic copies of it; (b) include such copies in the archives and digital repositories of the University; and (c) make freely available such copies to third parties for research or educational purposes after:

One ---- year from the date of submission of my thesis, dissertation, or project.

Two ---- years from the date of submission of my thesis, dissertation, or project.

Three ---- years from the date of submission of my thesis, dissertation, or project.

Hasan. H March 10, 2020

Signature Date

ACKNOWLEDGMENTS

I wish to thank Dr. Ghassan Dbaibo, who took me on as a thesis student, and whose patient and trusting philosophy, and immaculate shrewdness, created an auspicious environment where complex experimentation can be undertaken comfortably.

I wish to thank my supervisor Dr. Lina Reslan, who taught me to bring my A-game to the laboratory *each and every time* in order to maintain control, and who spent much time overseeing my experiments, correcting my thesis, and answering my inquiries.

I wish to thank Dr. Nadine Darwiche, Dr. Firas Kobaissy, and Dr. Hassan Zaraket for taking the time to serve as committee members, and for assisting considerably with their questions and insights.

I wish to thank Mr. Amer Sakr and Mr. Osama Yamani of AUST for their collaboration, and for their assistance in all matters pertaining to liquid chromatography and mass spectrometry.

I wish to express my appreciation for the labs of Dr. Matar and Dr. Zaraket for their friendly outreach when circumstances required a helping hand.

I wish to express my heartfelt gratitude to Dr. Nadine Darwiche, who guided me so elegantly and optimistically during my transition from banking/finance into biochemistry.

I wish to thank Dr. Marguerite Mrad and Dr. Rouba Hage-Sleiman for their accessibility and for contributing in great respects to my scientific edification.

I wish to thank the research assistants Marc and Nancy for their perennial eagerness to extend assistance and answer any laboratory inquiries.

I would like to express my gratitude to my DTS friends for their daily reinforcement and repartee, which generated much camaraderie.

I wish to thank lab manager Amjad Haidar, whose confidence, wit, and uniquely amiable humor positively grounded my research experience.

I wish to express my gratitude to my extraordinary friends - Lukas, Rola, Denise, Daniel, Bettina, Tristan, Allison, George, Danny, Taha, Pegor, Samuel, Sara, Wael, Ahmed, Yara, Tamara, Ameer, Timothy, Bernard, Dalia, Eyad, Makram, Paul, Caleb, and Hannah.

Lastly, I could not have transitioned into biochemistry and completed a master's degree without my endearing family serving as my transformative cocoon. A melancholic gratitude is deserved for my late cat, whose companionship flooded my home with a transcendent joy.

AN ABSTRACT OF THE THESIS OF

Hasan Mohamed Hijazi for Master of Science
Major: Biochemistry and Molecular Genetics

Title: Sphingolipidomics of Adenovirus-Infected Human Lung Adenocarcinoma Cells

Introduction: Human Adenoviruses (HAdVs) are obligate intracellular organisms that typically subvert epithelial cells by converting them into virion-producing factories. HAdVs encode a protein within the E3 region, termed adenovirus death protein (ADP), which facilitates cell lysis at the end of the viral cycle, thereby enhancing the dissemination of progeny virions via an unknown mechanism. Sphingolipids, a diverse pool of structural and bioactive lipids, are known mediators of various cellular pathways. One class of sphingolipids, ceramides, have an established role in the apoptotic cellular response to stress and were shown to be synthesized *de novo* shortly prior to cell lysis induced by wild type adenoviral infection. However, in cells infected with the E3-deleted mutant counterpart (dl7001), total ceramide, as measured by the diacylglycerol kinase assay, accumulated similarly but cell lysis did not occur due to the lack of ADP. Our current aim is to investigate the dynamics of sphingolipid changes induced by wild-type HAdV (*rec700*) and its E3-deleted mutant counterpart (*dl7001*) infection of A549 human lung adenocarcinoma cells by using Liquid Chromatography Tandem Mass Spectrometry (LC-MS) in order to understand the distinct cellular responses to these two viruses.

Methods: Cell viability was assessed by trypan dye exclusion. Analysis of cellular and viral gene expression was performed by real time PCR. LC-MS was performed on mock-infected cells, in addition to cells infected with either *rec700* or *dl7001*. Western blotting was used to assess the expression levels of dihydroceramide desaturase.

Results: Differential patterns of sphingolipid biosynthesis were observed in *rec700*- and *dl7001*-infected A549 cells. Whereas dihydroceramides accumulated significantly only in *rec700-infected cells,* ceramides accumulated significantly only in *dl7001*-infected cells.

Conclusion: We speculate that an E3 protein is interfering in the final step of the *de novo* synthesis pathway undertaken by the enzyme that converts dihydroceramide into ceramide.

CONTENTS

ILLUSTRATIONS

Figure Page

TABLES

Table Page

ABBREVIATIONS

ADP: Adenoviral death protein

Bak: Bcl-2 homologous antagonist/killer

Bax: Bcl-2-associated X protein

Bcl-2: B-cell lymphoma 2 protein

CAR: Coxsackievirus and adenovirus receptor

CerS: Ceramide synthase

cPLA2: cytosolic phospholipase A2

CtBP: C-terminal binding protein

DBP: Adenovirus DNA-binding protein

DEGS: Degenerative spermatocyte homolog (also known as ‘dihydroceramide desaturase’)

FIP: Fourteen.7k-interacting protein

KDSR: 3-ketodihydrosphingosine reductase

LCMS: Liquid chromatography / Mass spectrometry

MAD2B: Mitotic spindle assembly checkpoint protein

MHC: Major histocompatibility complex

MRN complex: Mre11-Rad50-Nbs1 complex

mTOR: Mammalian target of rapamycin

NF-κB: Nuclear factor kappa-light-chain-enhancer of activated B cells

p300/CBP: p300/CREB-binding protein

p400/TRRAP: p400/Transformation/transcription domain-associated protein

POD: Promyelocytic leukemia (PML) oncogenic domain

PP2A: Protein phosphatase 2A

pTP: Adenovirus precursor terminal protein

pRB: Retinoblastoma protein

RID complex: Receptor internalization and degradation (RID) complex

S1P: Sphingosine-1-phosphate

SPT: Serine palmitoyltransferase

SR proteins: Serine and arginine-rich (SR) proteins

TF(II): Transcription factor II

TNF: Tumor necrosis factor

TRAIL: TNF-related apoptosis-inducing ligand

CHAPTER I

INTRODUCTION

A. Human Adenoviruses

Adenoviridae (Ads) are non-enveloped DNA viruses first discovered in a human adenoid tissue sample in 1953 [1]. Ads infect most vertebrates [2] and, due to their diversity, have been grouped into six genera based on evolutionary similarities and DNA homology. Human adenoviruses (HAdVs), which belong to the Mastadenovirus genus, are comprised of 7 distinct species (HAdV-A to HAdV-G) that contain over 100 types in total (NIH's GenBank http://hadvwg.gmu.edu/). These viruses replicate their genomic content in the nucleus, where viral assembly also takes place, and the subsequent cell lysis leads to the release of progeny virions. Only one third of HAdVs are associated with disease [3], and >80% of HAdV infections occur in children <4 years of age [3]. Infection with different types of HAdVs may cause a range of illnesses from relatively mild infections such as conjunctivitis [4], acute gastroenteritis [5], acute respiratory infections (ARI) [6], to potentially fatal pneumonia [7]. HAdV infections have even been linked to the development of obesity [8]. HAdVs may also act as 'opportunistic infection' agents in immunocompromised individuals, leading to severe symptoms [9]. HAdVs are most commonly transmitted via respiratory routes [10] and can rapidly spread and cause outbreaks, albeit infrequent ones. The self-limiting nature of HAdV infections results in an underrepresentation in epidemiological data; data from the U.S indicates roughly 2,000 tested cases per decade [10, 11]. Exact figures on total mortality burden have not yet been

established established. HAdV vectors are highly popular in basic research, as they are produced at high titers, and are amenable to genetic engineering. Thus, HAdVs have become central to therapeutic applications such as *gene therapy [12]* and *virotherapy* [13, 14] for the past 60 years, and numerous clinical trials have been conducted [13]. HAdV2 and HAdV5, both belonging to species C, are the most widely studied serotypes.

1. HAdV Structure

The structure of HAdV is that of a nucleocapsid, consisting of nucleic acids surrounded by an icosahedral protein shell, termed the capsid. The complete virion is composed of 13 proteins (Proteins II, III, IIIa, IV, IVa2, V, VI, VII, VIII, IX, X, terminal protein TP, and the 23K protease), 7 of which serve structural capsid roles, while 6 localize in the virion's core and serve non-structural functions [15, 16] (Figure 1). Proteins II, III, and IV form the hexon, penton base, and fibre structures, respectively, while proteins IIIa, VI, VIII, and IX serve as capsid stabilizers that reduce the virion's sensitivity to mechanical and thermal stress. The 3 highly basic proteins V, histone-like protein VII, and X are located in the virion's core, non-covalently bound to DNA, whereas the terminal protein TP, also in the core, is tethered covalently at 5' ends of the viral genome. Another core protein, IVa2, aids in packaging the genome in the capsid. The 23K adenoviral protease, on the other hand, serves functions downstream during the infection process. The copy-numbers for each of the 13 proteins present in HAdV capsids have been established [17, 18]. Finally, roughly 27 other viral proteins are expressed *de novo* upon viral gene expression in the host cell, serving functions conducive to a successful infection (See: HAdV Genome Organization).

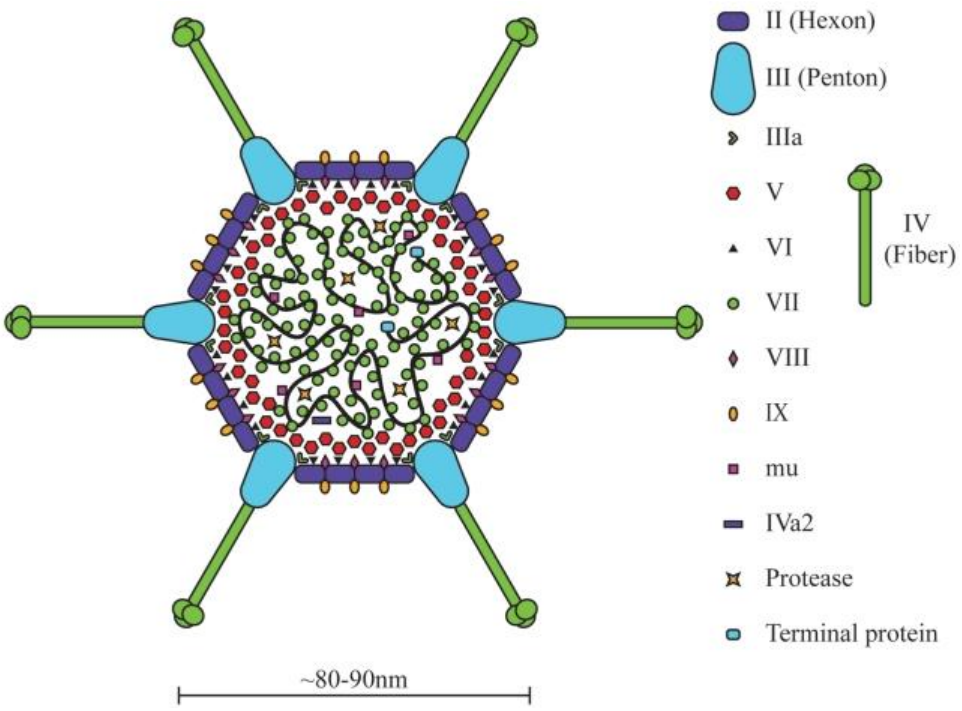

Figure 1: Schematic diagram HAdV nucleocapsid structure. 7 proteins collectively form the icosahedral capsid structure, while 6 proteins localize in the virion's core and serve non-structural roles. Image has been modified [19]

2. HAdV Entry and Nuclear Transport

HAdVs utilize multiple cell-surface receptors for entry, and each mode is dependent on the invading serotype. The most widely adopted entry mechanism is explained in this section. The HAdV *fiber* possesses a distal knob that attaches onto the transmembrane protein coxsackievirus and adenovirus receptor (CAR) [20], termed so in light of its capacity to accommodate binding by both HAdVs and coxsackie B viruses. Under normal conditions, CAR's activities include, but are perhaps not limited to, cell-cell adhesion in epithelial cells [21]. This initial binding allows an arginine-glycine-aspartate (RGD) loop

within the HAdV *penton* to bind to cellular α_V integrins [22]. These events subsequently initiate clathrin-mediated endocytosis [23], resulting in the invagination and entry of the HAdV in a vesicle-bound form. After entry, a partial disassembly of the capsid (termed 'uncoating') occurs via the activation of the previously-dormant adenoviral protease, owing to the cell's reducing environment [24]. The action of the protease leads to the release of capsid proteins [25], among which protein VI fractures the endosomal membrane, allowing the virion to escape into the cytoplasm where it is subsequently trafficked along the microtubule network towards the nucleus [26]. At the nucleus, Histone 1 escorts the viral DNA-protein complex through the nuclear pore [27], and viral gene expression begins shortly afterwards (figure 2).

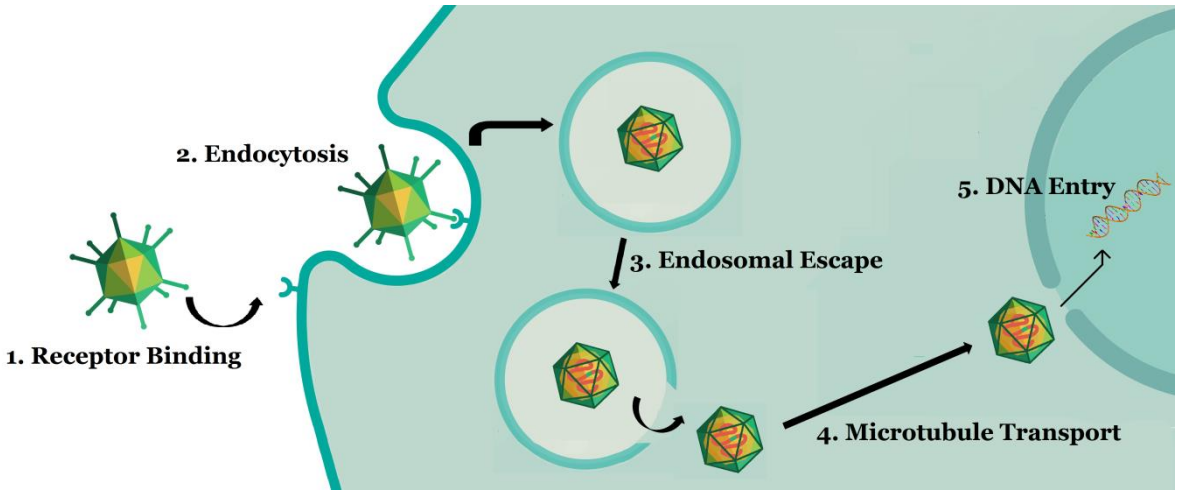

Figure 2: Schematic representation of HAdV attachment and internalization: The virion first binds to transmembrane proteins, namely CAR and integrins, followed by clathrin-mediated endocytosis. The virion escapes the endosome and, utilizing dynein-mediated microtubule transport, reaches the nucleus where it deposits its DNA. This image has been modified (Neuroscience: Canadian 1st Edition).

3. HAdV Genome Organization

HAdVs contain a single molecule of linear, double-stranded DNA that is roughly 36 kilobase pairs long. The genome is dichotomized into 'early' and 'late' genes, named on the basis of their expression before or after viral DNA replication, respectively. Cellular RNA polymerase II is required for transcribing the majority of HAdV genes [28], while RNA polymerase III is required for transcribing two viral non-coding RNAs [29]. In general, there are six early transcription units (E1A, E1B, E2A, E2B, E3, and E4), two intermediate units (IX and IVa2), and one late unit (Figure 3). Very soon after viral DNA enters the nucleus, an organized cascade of transcriptional events follows afterwards [30], culminating in the expression of roughly 40 different viral proteins.

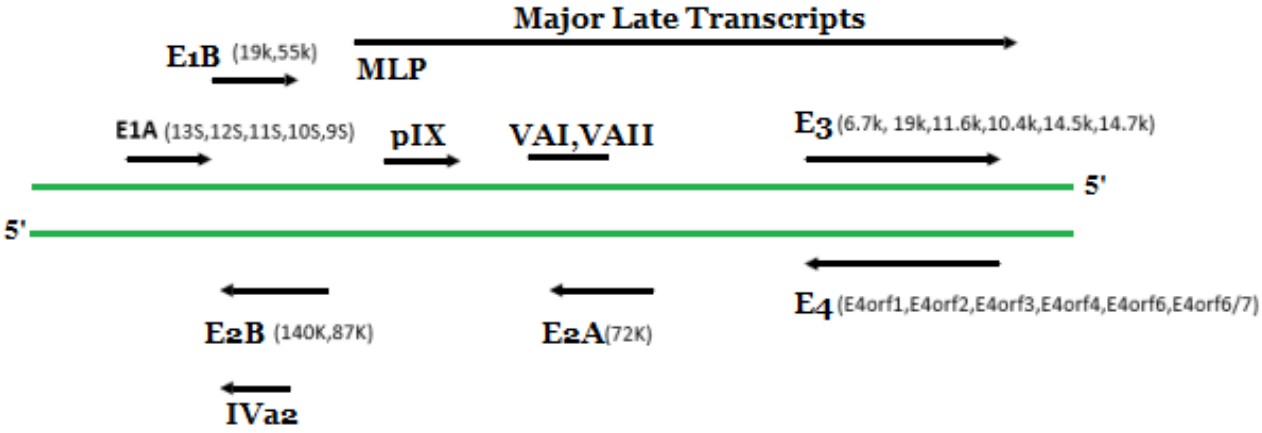

Figure 3: Schematic representation of the HAdV-5 genome. Transcription occurs on both strands of the viral genome, predominately via RNA polymerase II. A total of 10 transcription units (shown in bold) are transcribed which, due to splicing and polyadenylation options, generate a wide assortment of viral mRNAs. The direction of transcription for each unit is depicted by an arrow.

a. Early Gene Expression

i. E1A Unit

A total of five mRNA species are expressed from the E1A gene: 9S, 10S, 11S, 12S, and 13S. The proteins corresponding to the 12 and 13S variants, 243R and 289R respectively, will be addressed, as they carry out the majority of E1A's functions [31]. During HAdV infection, 243R and 289R proteins are the first to be expressed, localizing primarily in the nucleus [31] where they interact with roughly 32 cellular proteins [31]. The 46 amino acid difference between the two isoforms, corresponding to a conserved region (CR) termed CR3, activates the transcriptional machinery TF(II) and Sur2 [31], which subsequently trans-activates the expression of other viral early genes [32, 33]. Both E1A proteins are able to bind to hypo-phosphorylated retinoblastoma protein RB, which causes the release of transcription factor E2F [34, 35] and shifts the cell into the S-phase [36]. Additionally, E1A proteins massively deregulate cellular transcription via their interactions with p400/TRRAP-containing chromatin remodeling complexes [37], the C-terminal binding proteins (CtBP) [38], and p300/CBP [39, 40].

ii. E1B Unit

A total of four mRNA species are expressed from the E1B unit: 13S, 14S, 14.5S, and 22S [41, 42]. 22S and 13S are the most abundant variants (95% of total) [43], and are translated into 19K and 55K proteins, respectively. The function of E1B is to subvert the pro-apoptotic signaling elicited by E1A proteins, which were shown to induce an accumulation of p53 [44, 45] and sensitize the host cell to lysis by TNF (*in vivo*) [46]. The anti-apoptotic

effects of E1B lead to a lengthened infection, and a successful entry into the late phase. 19K is a homologue of the cellular Bcl-2 protein [47, 48], which inhibits apoptosis by inhibiting Bak/Bax-mediated permeabilization of the outer mitochondrial membrane, thereby causing a retention of pro-apoptotic proteins in the mitochondria [49]. On the other hand, 55K directly binds to the N-terminus of p53 and inhibits its transcriptional activity [50]. Moreover, by forming a complex with E4orf6, 55K is also able to target p53 proteins for degradation (See: E4orf6). In addition to its anti-apoptotic role, 55K mediates the translocation of late viral mRNAs from the nucleus to the cytoplasm [51] and inhibits the translation of non-viral proteins [52].

iii. E2A and E2B Units

The E2 gene corresponds to the virion's built-in genomic replication machinery. This gene is transcribed into two classes of transcripts termed E2A and E2B [53, 54]. E2A generates the single-stranded DNA-binding protein (DBP), whereas E2B generates the terminal protein (pTP) and the adenoviral polymerase (Adv-Pol). pTP functions as a viral-DNA primer, and Adv-pol elongates a nascent strand via its 5' to 3' polymerase activity in addition to a 3' to 5' proofreading activity [55-57]. DBP, on the other hand, not only protects ssDNA during the elongation process [58], but also partakes in the assembly of virion particles during the final stages of the lytic cycle [59].

iv. E3 Unit

The E3 unit is mostly implicated in *in vivo* immunomodulation [60], and is completely dispensable *in vitro* [61]. Nine mRNAs are generated from the E3 gene [62], and 7 proteins have been identified: 6.7K, 10.4K, 11.6K, 12.5K, 14.5K, 14.7K, and 19K [63-69]. 12.5K is not essential for viral replication, and its function is still unknown [66].

6.7K is a membrane protein that localizes primarily in the ER [63, 70], but may also localize at the plasma membrane where it interacts with the receptor internalization and degradation (RID) complex (which will be addressed shortly) [71]. 6.7K, via its interaction with RID, downregulates TNF-related apoptosis-inducing ligand 2 (TRAILR2) [71], and perhaps TRAILR1 as well [71]. In the ER, 6.7K represses apoptosis via a mechanism involving cytosolic calcium homeostasis [72].

10.4K (RIDα) and 14.5K (RIDβ) proteins uniquely interact and form the RID complex [73]. RID localizes at the plasma membrane [74, 75], although RIDα displays a Golgi localization and RIDβ displays an ER/Golgi localization when these proteins are not in their complex form [74, 75]. As the name implies, RID stimulates the internalization and degradation of several membrane receptors such as Fas [76], TNF-related apoptosis-inducing ligand 1 (TRAILR1) [71, 77], TRAILR2 [71], and perhaps tumor necrosis factor receptor 1 (TNFR1) [78]. Additionally, RID stimulates the downregulation of several tyrosine kinase receptors such as the epidermal growth factor receptor [73, 79]. Moreover, RID inhibits the immune response by prohibiting the nuclear entry of transcription factor NF-κB [78].

11.6K, also known as ‘Adenoviral Death Protein’ (ADP), is a lytic protein unique to group C HAdVs. ADP is a membrane protein [80] that displays a time-dependent

localization, initially localizing in the Golgi, then re-localizing to the ER, and finally localizing at the nuclear membrane [80]. This protein is produced only in miniscule amount in the early stage, but becomes much more expressed in the late stage [81]. ADP promotes the efficient release of virions from the cell at the end of the infectious cycle [82]. ADP interacts with a cellular protein termed mitotic arrest deficiency 2B (MAD2B) [83], otherwise known as MAD2L or hREV7. The lytic capacity of ADP is dependent upon its ability to counteract the function of MAD2B, although the mechanisms and consequences of this interaction are largely unknown.

14.7K localizes in the cytoplasm and the nucleus [84, 85]. This protein inhibits the extrinsic apoptosis pathway mediated by tumor necrosis factor (TNF) [84, 86], and therefore inhibits TNF-induced activation of cytoplasmic phospholipase A2 and the subsequent release of arachidonic acid [87, 88]. 14.7K interacts with several cellular proteins termed fourteen.7K- interacting proteins (FIPs) [85, 89, 90]. FIP-1 is a protein that interacts with dynein [91], which suggests a role for 14.7K in nuclear-cytoplasmic trafficking. FIP-2, on the other hand, is a Golgi protein that is re-localized to perniculear structures in the presence of 14.7K [85]. FIP-3 is an inducer of NFkB signaling [92-94]. Although originally localizing in the cytoplasm and the nucleus, FIP-3's localization becomes confined to perinuclear structures in the presence of 14.7K [89]. The relevance of 14.7K's interaction with FIPs is largely unknown.

19K is a glycoprotein that anchors predominantly to the endoplasmic reticulum [95]. During *in vivo* viral infection, if viral peptides are presented on the plasma membrane of the host cell *via* major histocompatibility complex class I molecules, this would trigger a

$CD8^+$ T cell-mediated destruction of the infected cell. HAdVs are able to mitigate against this via 19K's binding to the peptide-displaying MHC class I molecules, thereby hindering their transport to the plasma membrane [96]. A similar sequestration mechanism by 19K also results in the evasion of natural killer cells [97].

v. E4 Unit

The E4 region possesses one promoter and is transcribed into a single primary transcript which, upon alternative splicing, generates 24 mRNAs [98, 99]. However, only 6 proteins have been described: E4*orf*1, E4*orf*2, E4*orf*3, E4*orf*4, E4*orf*6, and E4*orf*6/7. The functions of E4*orf*2 are still unknown.

E4*orf*1 binds to and activates the transcription factor MYC [100], leading to the upregulation of glycolytic genes. Interestingly, this increased glycolysis upregulates nucleotide synthesis *via* metabolic flux into the pentose phosphate pathway [100]. These nucleotides are necessary for viral genomic replication during the late phase.

E4*orf*3 mainly associates with the nuclear matrix [101]. This protein induces a structural change in promyelocytic leukemia (PML) oncogenic domains (PODs) [102], which are intra-nuclear structures that regulate transcription, apoptosis, DNA repair, genomic stability, transformation, and viral replication [103]. E4*orf*3 sequesters the Mre11-Rad50-Nbs1 (MRN) complex in these PODs; an event that subverts the DNA-damage response against the virus [104]. E4*orf*3 also possesses SUMO E3 ligase activity, which has been implicated in the re-localization of many cellular proteins [105].

E4*orf*4 interacts with the phosphatase PP2A [106] and the kinase Src [107]. Via PP2A, E4*orf*4 mediates the de-phosphorylation of a sub-set of SR proteins [108], namely SF2/ASF and SRp30c [109], leading to increased alternative splicing of viral and cellular

genes. Also via PP2A, E4*orf*4 activates the mTOR pathway [110], which is necessary for S-phase entry [111]. The interaction between E4*orf*4 and Src leads to the former's Tyr phosphorylation and subsequent re-localization from the nucleus to the cytoplasm.

E4*orf*6 binds to the C-terminus of p53 and inhibits its transcriptional activity [112]. Additionally, E4*orf*6 forms a complex with E1B-55K that shuttles between the nucleus and the cytoplasm [113]. This complex mediates the cytoplasmic transport of late viral mRNAs, while simultaneously preventing the transport of cellular mRNAs [114, 115]. Moreover, this complex mediates the poly-ubiquitination and proteasomal degradation of p53 via its ubiquitin ligase activities [116, 117].

The only known function of E4orf6/7 is its recruitment of transcription factor E2F/DP to the promoter of the viral E2 gene, leading to this gene's transactivation [118, 119].

b. Intermediate Gene Expression

Two proteins, IX and IVa2, are expressed around the time of viral genomic replication [120, 121]. The function of these 2 proteins is described above (See: HAdV Structure).

c. Late Gene Expression

During the late phase, the activation of the major late promoter (MLP) leads to the generation of a single transcript (~28,000 nucleotides long) from the major late transcription unit (MLTU) and the subsequent generation of 5 late families of mRNAs (L1-L5). The MLTU generates ~20 mRNAs. The MLTU is actually activated during the *early*

phase of infection as well, but only a truncated expression of this unit is observed at that time, yielding the L1 52,55K mRNA [122]. Moreover, during an 'intermediate' phase of infection prior to the late phase, it was shown that L4-22K and L4-33K proteins are expressed from a novel L4P promoter [121].

The L1 unit generates 3 proteins: 52K, 55K and IIIa. The function of IIIa is described above (See: HAdV Structure), and the 52/55K proteins aids in virion capsid assembly [123, 124].

The L2 unit generates 4 proteins: III, V, VII, and X [125, 126]. The function of protein III is described above (See: HAdV Structure). Protein VII protects the viral DNA from a cellular DNA-damage response during the initial stages of viral infection [127], whereas protein V serves to bridge a connection between the virion's DNA and its capsid [2]. The function of protein X is still unknown.

The L3 unit generates 3 proteins: III, VI, and the adenoviral protease [128]. The function of III and VI is described above (See: HAdV Structure). The protease, which possesses cysteine endopeptidase activity, is important for capsid maturation, cleaving 6 capsid proteins (IIIa, VI, VII, VIII, X, and TP) into their mature counterparts [129] in a process termed 'capsid priming'.

The L4 unit generates 4 proteins: 22K, 33K, 100K, and VIII [130]. L4 is transcribed via two different promoters, L4P and MLP, depending on the time of infection, whereby L4P is first activated by E1A, E4*orf*3, IVa2, and p53 [121, 131]. Upon L4P activation, two of the expressed proteins, 22K and 33K, generate a feedback loop that triggers the complete activation of MLP [132], culminating in the initiation of the late phase. 22K and 33K proteins mostly partake in virion assembly [133, 134], whereas 100K promotes the

selective recruitment of ribosomes to viral *late* mRNAs, and thus significantly reduces cellular mRNA translation in the process ('ribosomal shunting') [135]. The function of protein VIII has been previously described (See: HAdV Structure).

The L5 unit generates a single protein, IV, the function of which is described above (See: HAdV Structure).

4. HAdV-Induced Cell Lysis

The mechanism by which HAdVs induce cell lysis is largely unknown. The adenoviral death protein (ADP) of the E3 gene has been largely implicated in host cell lysis, but is interestingly also dispensable in all regards. For instance, an HAdV mutant that overexpresses ADP was shown to significantly enhance the rate of cell death without reducing net viral yield [136]. However, HAdV mutants that do not express ADP were still able to induce lysis, albeit in a delayed manner and with reduced dissemination capacity [82, 136, 137]. Alternatively, a previous study from our laboratory demonstrated that HAdV infection induced a significant accumulation of *de novo* synthesized ceramide prior to the commencement of cell death, and that the inhibition of ceramide synthesis resulted in the delay of cell death onset [138]. Since 'ceramide' is not a single molecule but is rather a group of closely related but distinct species that induce differential biological effects, the subsequent section will review ceramides and sphingolipids in general.

B. **Sphingolipids**

Cellular lipids have been estimated to be in the order of 200,000 molecules [139], and are grouped into eight classes [140]. One of these classes, the "sphingolipids", entails thousands of molecules that serve as major membrane components [141] and regulators of cell growth, apoptosis, differentiation, migration, autophagy, cell-cell/cell-matrix interactions, and others [142, 143].

1. Sphingolipid Structure and Nomenclature

Sphingolipids are characterized by the *sphingoid* backbone feature, which is an alkane or alkene that contains hydroxyl-constituents at positions 1 and 3, and an amino group at position 2. A meta-structure containing three variable regions has been provided (figure 4). Variable *A*, the aliphatic chain of the sphingoid backbone, varies in length, degree of unsaturation, branching, and may contain an additional hydroxyl group. Variable *B* is an acyl chain that typically ranges from 14 to 26 carbons, may contain between 0 to 6 double bonds, and may be branched or modified (oxygenated, nitrated, etc.). Variable *C* may be hydrogen or a polar head group, the latter of which generates glucosylceramides, lactosylceramides, sphingomyelins, and others. Examples of key sphingolipid structures have been provided (figure 5).

A system of nomenclature has been developed to distinguish each sphingolipid. d18:0/14:0, for instance, represents a sphingolipid containing 2 hydroxyl groups (d for 'di'; t for 'tri') in the main aliphatic chain (18:0 indicating that this chain is 18 carbons in length, and has 0 double bonds), and a saturated 14-carbon (14:0) N-acyl derivative.

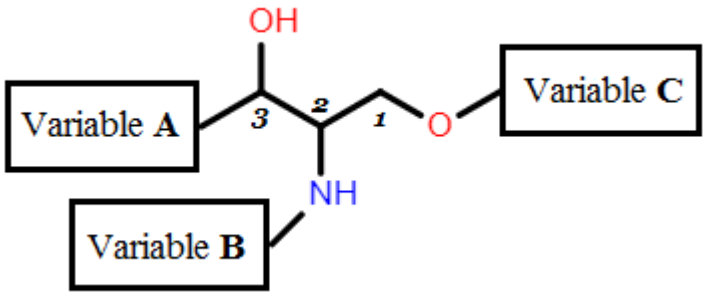

Figure 4: Schematic of sphingolipid meta-structure. A sphingoid backbone (Variable A), containing hydroxyls at positions 1/3 and an amino group at position 2 is common to all sphingolipids. Additional conjugations (Variables B and C) increase the diversity of sphingolipid species in a combinatorial manner.

2. Sphingolipid Metabolism

Roughly 40 enzymes coordinate the sphingolipid metabolism network, and each enzyme has a unique subcellular localization and may re-localize *via* post-translational modification. In most cases, the sphingolipid products remain in their area of generation unless transported to a different sub-cellular location. Many of the key pathways have been provided (figure 6).

a. *De novo* Ceramide Synthesis

The *de novo* pathway, which is the entry-point into sphingolipid biosynthesis, takes place in the endoplasmic reticulum (ER). Four reactions conducted by 4 membrane-bound enzymes generate ‘ceramides’, a diverse class of molecules that serve as core building blocks for generating more complex sphingolipids.

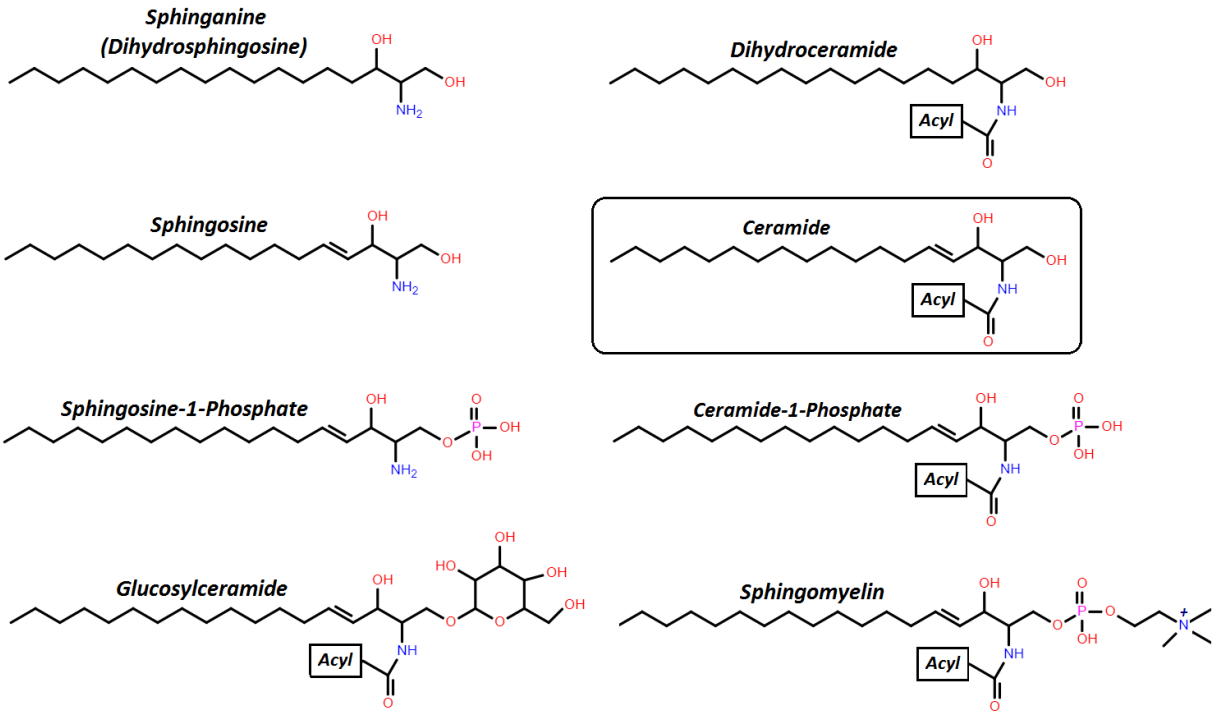

Figure 5: Key sphingolipid structures. N-acylation is represented as a box containing the term "acyl", and the length of this acyl chain may vary considerably. The simplest sphingolipids are sphinganine/sphingosine, followed by dihydroceramide/ceramide. They may be conjugated with polar head groups at the C1-hydroxy position, thereby generating more complex sphingolipids such as sphingosine-1-phosphate (in the case of sphingosine), ceramide-1-phosphate, sphingomyelin, glucosylceramide, and lactosylceramide.

The *de novo* pathway begins by the activity of *serine palmitoyl transferase* (SPT), a heterodimer of SPT1 and SPT2 [144] that condenses L-serine and palmitoyl-CoA to form 3-ketosphinganine. *3-ketosphinganine reductase* (KDSR) then generates sphinganine, which is subsequently N-acylated by one of 6 *ceramide synthases (CerS)*, yielding dihydroceramide [145]. The 6 mammalian ceramide synthases each possess a specificity in the length of the acyl chain by which they acylate sphinganine [146] (Figure 7).

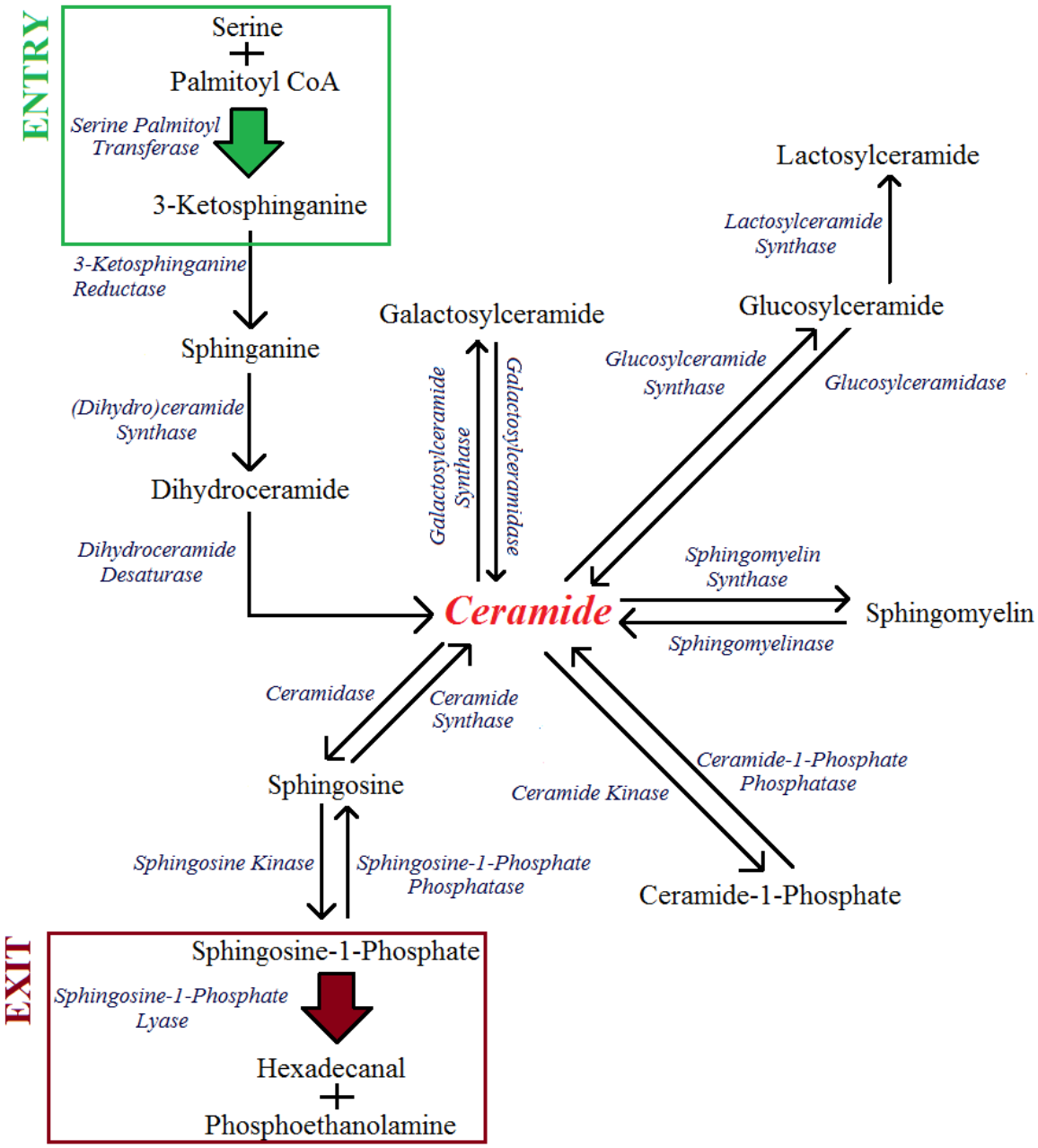

Figure 6: Schematic of the sphingolipid metabolic network. The *de novo* pathway serves as an entry point (green box) into sphingolipid biosynthesis, and generates the hub molecule 'ceramide'. Ceramide may then act as a substrate for the generation of sphingomyelin, glycosphingolipids, and ceramide-1-phosphate. Ceramide may also be broken down into sphingosine which, via the subsequent actions of sphingosine kinase and sphingosine-1-phosphate lyase, leads to the exit pathway (red box). This figure represents a 'generic' depiction of sphingolipid metabolism, as it does not show the subcellular localizations, diversity is sub-species, or the fact that dihydroceramide itself may also serve as a substrate in many of the pathways partaken by ceramide.

In the final step of *de novo* ceramide synthesis, the enzyme *dihydroceramide desaturase* (DEGS) generates a Δ4,5 double bond [147], culminating in the formation of 'ceramides'. After its generation, ceramide may be channeled into one or more of the pathways depicted in figure 6, depending on its transport and the availability/activity of subsequent enzymes and substrates.

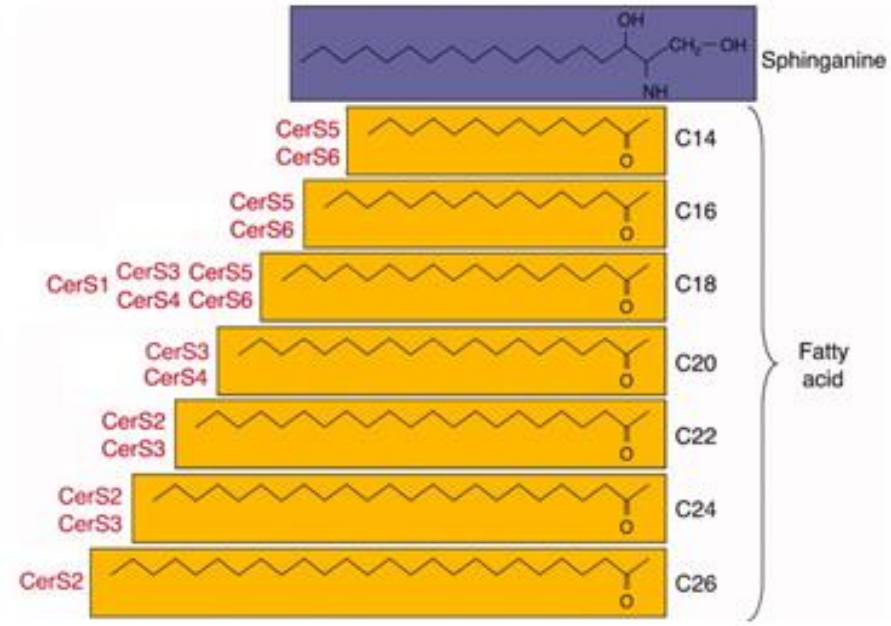

Figure 7: Schematic of ceramide synthase (CerS) activities. 6 mammalian ceramide synthases (red) have been characterized, each displaying a unique N-acylation fingerprint [145]. Ceramide synthases convert sphinganine or sphingosine into dihyroceramide or ceramide respectively via the incorporation of an acyl chain ranging in length from 12 to 34 carbons (although the most common ones are those depicted in the figure). More than 20 acyl chains are potentially available, varying in chain length, degree of unsaturation, and hydroxylation. There is some conflicting data regarding the exact acyl chain specificities of each ceramide synthase, and this figure represents the most common affinities of these enzymes.

b. Post-*De Novo* Sphingolipid Metabolism

'Complex' sphingolipids are ceramides (or dihydroceramides) that have been conjugated with a polar head group at the C1-hydroxy position. These sphingolipids are generated in the Golgi, and ceramides must first make their way from the ER to the Golgi, doing so either via ceramide transfer protein (CERT) or vesicular transport [148]. In the Golgi, ceramides are metabolized into sphingomyelins via *sphingomyelin synthase*, glucosylceramides vis *glucosylceramide synthase*, galactosylceramides via *glactosylceramide synthase*, lactosylceramides via *lactosylceramide synthase*, and ceramide-1-phosphates via *ceramide kinase* [142, 149]. Other highly complex metabolites such as gangliosides are also generated in the Golgi, mostly from lactosylceramide as a precursor [150].

In the plasma membrane, sphingomyelins may be hydrolyzed into ceramide via the action of *neutral sphingomyelinase* or *acid sphingomyelinase* in the inner leaflet or the outer leaflet, respectively [142]. The majority of sphingomyelins, however, are localized at the outer leaflet.

Several sphingolipid metabolism pathways have been grouped under the 'salvage pathway', which takes place in the endo-lysosomal compartment. 'Salvaging' includes the breakdown of complex sphingolipids into ceramides, the breakdown of ceramides into sphingosine, and the conversion of sphingosine into ceramides [151].

3. Biological Effects of Sphingolipids

Ceramides have emerged as key players in the induction of growth arrest and cell death [152] , whereas sphingosine-1-phosphate (S1P) has been recognized as an enhancer of cell survival and proliferation [153]. The balance between ceramides and S1P was initially believed to determine the cell's fate, in what was termed the "sphingolipid rheostat". However, an extensive characterization of sphingolipid metabolism has suggested that this two-dimensional model is not consistently representative of sphingolipid signaling. Moreover, the bioactive nature of sphingolipids proved to be even more complex in the context of dihydroceramides. Initial experiments using cell permeable ceramides and dihydroceramides showed that the double bond in the sphingoid base was crucial for the bioactivity of these sphingolipids, since the dihydroceramide counterparts induced no apoptotic effects [154, 155]. This led to the conclusion that dihydroceramides were inert molecules that played no role in cellular signaling. However, this paradigm has begun to change considerably in recent years, as many studies reported the induction of an autophagic cellular response upon the inhibition of DEGS and the subsequent significant increase in dihydroceramides in the endoplasmic reticulum [156-158]. This dihydroceramide-induced autophagic response was shown to induce cancer cell death in certain cases [159]. Additionally, the specific compartmental generation or degradation of sphingolipids influences the type of cell death that occurs [160, 161]. This final aspect adds a compartmental layer to the complexity of sphingolipid bioactivity.

CHAPTER II

THESIS OBJECTIVES AND AIMS

Previous work from our group demonstrated that adenovirus-infected MCF-7 cells accumulated ceramide starting at 24 hours post-infection, followed by their lysis several hours later. The ceramide was shown to be synthesized *de novo* and appeared to be implicated in adenovirus-induced cell lysis, as the *de novo* pathway inhibitors Myriocin and Fumonicin B abrogated the aforementioned accumulation and delayed cell death by roughly 12 hours. On the other hand, MCF-7 cells infected with an adenovirus mutant lacking all the E3 genes, *dl7001,* similarly accumulated ceramide at 24 hpi, but did not undergo cell lysis within the span of 48 hours [158]. This dissociation of ceramide accumulation from subsequent cell lysis prompted us to investigate the role of ceramide during adenoviral infection and its regulation by different adenoviral genes. We decided to utilize a sphingolipidomic approach using the highly sensitive LC-MS technology in order to identify any sphingolipid differences across both (*rec700* and *dl7001*) adenoviral-infected cells. Additionally, we applied real-time gene expression analysis of adenoviral genes and sphingolipid enzyme genes in order to identify a causal link to the sphingolipid alterations.

CHAPTER III

MATERIALS & METHODS

A. Cell line and adenoviruses

A549 human lung adenocarcinoma cells were grown as monolayers in Dulbecco's modified Eagle's medium (DMEM) supplemented with 10% (vol/vol) fetal bovine serum and 1% penicillin/streptomycin. Cells were maintained at less than 90% confluency under standard incubator conditions (humidified atmosphere, 95% air, 5% CO_2, 37ºC), and passaged 2-3 times weekly by trypsinization. *Rec700* is an HAdV5/HAdV2 recombinant consisting of HAdV5 sequences across map positions 0-76 and 83-100, and HAdV2 sequences ligated in between [162]. *Rec700* is considered a wild-type HAdV from which many mutants were generated. One such mutant, *dl7001*, lacks the entire E3 unit [163]. Both adenoviruses were a kind gift from Dr. William Wold (St Louis, MO).

B. Adenovirus titration

Plaque assays were performed as described by Green and Wold [164]. A549 cells were seeded at a density of 500,000 cells/well in six-well plates and incubated for 24 hours. Complete media was then removed, and cells were incubated in serum-free media for 30 minutes, during which serial dilutions (10^{-3} to 10^{-10}) of virus stock were prepared in serum-free media. For the first dilution (10^{-3}), 5µL of virus stock was pipetted into 5mL of serum-free DMEM, and a 10-fold sequence dilution was generated from there (until 10^{-10}). The media was pipetted out from the cells, and 400µL of the media/virus mixture was pipetted

into each well. Cells were incubated for 1 hour, during which plates were gently swirled every 10 minutes in order to ensure complete coverage of cells. The media was then removed, and 3mL of an overlay mixture consisting of melted agar gel (1.8% w/v), FBS (2% v/v), and DMEM was pipetted into each well. After solidification of the gel, the plates were incubated until cytopathic effect was visible under the microscope, after which 2mL of the same gel overlay containing neutral red dye (0.45% of a 3.33g/L stock solution) was added. Plaques, which correspond to zones of dead cells unstained by the dye, were counted ever day until no additional plaques were observed. The virus stock concentration was then calculated as such:

$$Virus\ titre = \frac{(Number\ of\ virus\ plaques) * (Dilution\ factor)}{Volume\ of\ applied\ virus\ solution\ (mL)}$$

C. Viral infections

One day prior to infection, cells were seeded in six-well plates at a density of 500,000 cells per well. The next day, complete media was removed, and cells were incubated in serum free media for 30 minutes at 37ºC. The media was subsequently removed, and cells were infected at a multiplicity of infection (MOI) of 40pfu/cell (plaque-forming units per cell) in 400µL of serum free media, during which plates were gently swirled every 10 minutes for 1 hour in order to ensure complete coverage of cells. After 1 hour, 2.5mL of complete DMEM was added to each well, and cells were incubated (t=0) until their respective harvest times at 6, 12, 24, 36, and 48 hpi. At the time of harvest, the media was transferred to falcon tubes, into which the trypsinized cells were subsequently

placed. Cells were pelleted by centrifugation (1,500 RPM, 5 min, 4ºC), after which the supernatant was discarded and fresh PBS was added. Cells were pelleted again by centrifugation, the supernatant was discarded, and samples were stored at -80ºC.

D. Trypan blue dye exclusion assay

The viability of A549 cells was measured by the exclusion of trypan blue dye, indicative of an intact plasma membrane. At the time of harvest, a 50µL volume of cells was diluted with an equal volume of 0.4% trypan blue dye, and cells were counted using a hemocytometer. The data represents the average of two independent experiments.

E. Protein Extraction and Quantification

Protein quantification was conducted for the purpose of phospholipid normalization. In short, cell pellets were mixed with appropriate amounts of protease inhibitors and lysis buffer (Tris-HCl, SDS 4%, glycerol 20%, and bromophenol blue 2mg) at a ratio of 1:25. Samples were then vortexed, placed on ice for 20 minutes, boiled at 95ºC for 5 minutes, and subsequently centrifuged (maximum speed, 4ºC, 20 minutes). The supernatant was then transferred to new eppendorfs, and proteins were quantified using the Lowry assay [165].

F. Western Blotting

Protein expression levels were analyzed using 12% acrylamide gels. Samples were prepared with a l:1 volume ratio of proteins to loading buffer [Tris-HCl 0.25 M (pH 6.8), 4% SDS, 20% glycerol, 2mg bromophenol blue, and 5% β-mercaptoethanol], and run using

tris-glycine-SDS buffer (TGS 1x). Migration was conducted at 80V for the stacking phase, and 120V for the resolving phase. Following migration, transfer to a polyvinylidene difluoride (PVDF) membrane was performed in a transfer buffer [TGS 1X with 20% methanol] for 90 minutes at 100V. The membrane was then blocked overnight at 4ºC in 5% fat-free milk prepared in tris-buffered saline (TBS1X) with 0.1% tween. Following blocking, the membrane was incubated overnight at 4ºC in 2mL of a primary antibody (polyclonal rabbit anti-DEGS and polyclonal rabbit anti-histone 3) diluted in 5% milk-TBS 1X containing 0.1% tween as recommended by the supplier. The membrane was then washed for 10 minutes with TBS 1X containing 0.1% tween in three cycles, and subsequently incubated at room temperature for 1 hour with horseradish-peroxidase (HRP)-conjugated secondary antibody diluted in 5% milk-TBS 1X containing 0.1% tween as recommended by the supplier. Finally, the bands were developed with enhanced chemiluminescence (ECL) western blotting reagent. For DEGS and Histone 3, a rabbit secondary antibody (1/5000 dilution) was utilized (Jackson).

G. RNA Extraction and Reverse-Transcription

Total RNA was extracted using the GenElute Mammalian Total RNA Miniprep Kit (Sigma Aldrich, USA) according to the manufacturer's instructions. Briefly, samples were lysed using a mixture of β-mercaptoethanol and lysis solution at a ratio of 1:100. Extracts were passed through a first filter via centrifugation, and equal volumes of 70% ethanol were subsequently added to the filtrate. The mixture was then passed through a second

column via centrifugation, and a series of wash steps was followed by elution of the RNA from the filter.

A 1µg volume of total RNA was reverse transcribed using the Quantitect Reverse Transcription Kit (QIAGEN, Germany) according to the manufacturer's instructions. Briefly, a 14µL mixture of RNA, nuclease-free water, and gDNA wipeout buffer was first incubated in a thermal cycler at 42ºC for 2 minutes. 6µL of a mastermix (reverse transcriptase, primer mix, and buffer) was subsequently added, and the samples were incubated at 42ºC for 30 minutes, followed by 95ºC for 3 minutes to deactivate the reaction. cDNA was then diluted to a final concentration of 10ng/µL, and was used for both conventional PCR and RT-PCR.

H. Gene Expression Levels by PCR

All viral primers were purchased from Macrogen (Table 1). Primers for E1A9S-13S have been previously described [166], and the remaining primers were designed using the DSgene program. Primers for sphingolipid metabolism enzymes have been previously optimized by our lab. Viral primers were temperature-optimized prior to RT-PCR, utilizing conventional PCR and gel electrophoresis. Conventional PCR was applied using the 2x PCRBIO HS Taq Mix Red (PCR Biosystems) according to the manufacturer's instructions. A 20µL mixture containing nuclease-free water, primers (reverse and forward), cDNA, and Taq Mix Red was incubated at 95ºC for 1 minute followed by a 40 cycle PCR reaction (95ºC 1 min, 55-63ºC 15 sec, 72ºC 90 sec). Amplified cDNA was loaded on a 2% agarose gel, along with a 50bp ladder (Sigma-Aldrich, USA), and electrophoresis proceeded at

100v followed by UV detection. The optimum temperatures were identified as 57ºC for E3-ADP, and 60ºC for all the remaining viral primers.

	Target	Forward Primer (5' - 3')	Reverse Primer (5' - 3')
Viral Genes	E1A-9S	TGATCGAAGAGGTCCTGTGTCT	TCAGGATAGCAGGCGCCA
	E1A-10S	GATCGAAGAGCCCGAGCA	GGAGTCACAGCTATCCGTACTACT
	E1A-11S	GATCGAAGAGCCCGAGCA	CCACAGGTCCTCATATAGCAAA
	E1A-12S	TTTTGAACCACCTACCCTTC	GGAGTCACAGCTATCCGTACTACT
	E1A-13S	TTTTGAACCACCTACCCTTC	CCACAGGTCCTCATATAGCAAA
	E1B-19K	GGCTCATCCCAGGCAAAGTTAG	TCAAACAGCTCACCACAGGATTTC
	E1B-55K	TGCTGGCGCAGAAGTATTCC	AATCTGGCCTAAGTGCCACC
	E2-DBP	TCTTGTTGCTGGTGAAGGTC	CAAACTACTGCCTGACCAAGTG
	E2-POL	TCTTCGGCATCAAGGAAGGTG	ATGCGGAAGAGAGTGAGGAC
	E2-PTP	GAAGAAGTACATAACCCAGCGTCG	ACTTCGCCGTGGACTTCTAC
	E3-ADP	CCCAAGTTTCTGCCTTTGTC	GCAGCAGATGAGCCACATAA
	E4*orf*3	GATGTTGCACAATGGCTTCC	TGGTTGAAGGTGCTGGAATG
	E4*orf*4	CACTCTCTCAAAGCATCCAGG	CTTATTCTGCGGTGGTGGATG
	E4*orf*6	CCCTCATAAACACGCTGGAC	GCTGGTTTAGGATGGTGGTG
	E4*orf*6/7	TCCCAACACACAGAGTACACAG	TTGGCTCGACAGAAACCGTG
Sphingolipid Enzymes	nSMase	CCTTTGCGTTTCTCGGCTTTC	CCCGTGCCCTTCCATTCA
	SPT1	AGGAGTCACTGAACACTATG	AGCTCTCTCCAGTTCTTCCT
	SPT2	CAAAGAGCTTCGGTGCTTCAG	GAATGTGTGCGCAGGTAGTCTATC
	CerS2	CCGATTACCTGCTGGAGTCAG	GGCGAAGACGATGAAGATGTTG
	CerS3	GCCCCACACCGACCCCACAT	AACAAAGCGAGCCCCTGAGAAAGT
	CerS4	CTTCGTGGCGGTCATCCTG	TGTAACAGCAGCACCAGAGAG
	CerS6	ACATTCCTTCAGCCTCCTGGAGTT	GCTCCCTGGTTTCCAGGCCAC
	DEGS1	CCAACATTCCTGGAAAAAGTCTTC	GCCTCTTCATTCTTGAGTAGGGA
	SphK1	CTGGCAGCTTCCTTGAACCAT	TGTGCAGAGACAGCAGGTTCA
	KDSR	ATGGGCCTTTTCCGCACTATTG	AGCCACATTCCTGAAGAGCACTG

Table 1: Primer sequences. The following is the comprehensive list of primers used for viral gene expression and sphingolipid metabolism enzyme expression.

For RT-PCR analysis of viral genes, cDNA amounts were first optimized by performing a serial dilution (10ng 20ng, 40ng) using the BioRad CFX96 real-time thermocycler. 20ng cDNA was chosen for all future RT-PCR reactions in order to minimize pipetting errors. All RT-PCR reactions were performed in 12µL reaction mixtures containing 6µL SYBR Green (Sigma-Aldrich, USA), 20ng cDNA, 250nM of forward/reverse primers, and nuclease-free water. Annealing temperatures for sphingolipid enzyme primers are 56ºC for sphingosine kinase, 59ºC for DEGS1, and 60ºC for all ceramide synthases. Annealing temperatures for viral primers were 57 ºC for E3-ADP and 60 ºC for all the rest. We have previously observed that GAPDH mRNA concentration remains steady in A549 cells infected with *rec700*, and we therefore normalized all genes to GAPDH. The delta Ct method was used for viral genes, whereas the delta-delta Ct method (Livak) was used for sphingolipid metabolism enzymes.

I. Lipid extraction and LC-MS

Total lipids were extracted as previously described [167]. Briefly, isotope-labeled internal standards were first added to the cell pellet, followed by the addition of a mixture of ethyl-acetate:isopropanol:water (60:30:10 [v/v/v/]). The samples were fully dispersed by sonication for 30sec and vortexing, and were centrifuged for 5 min at 3,000g. The organic upper phase was transferred to a new vial, and was subsequently dried under nitrogen. The dried residue was re-suspended in a mobile phase (1 mM of ammonium formate in methanol containing 0.2% formic acid) and centrifuged 5 min at 3,000g. The supernatant was then injected into a high performance liquid chromatography (HPLC) system, and lipids were differentially eluted.

Based on the isotope-labeled internal standards used, tandem mass spectrometry (MS/MS) was used in order to detect sphingosine, ceramides, sphingomyelins, glucosylceramides, lactosylceramides, and the dihydro-counterparts of each of these classes. The HPLC system is coupled to MS/MS containing a triple quadrupole as the mass analyzer. After eluting from the HPLC system, lipids were passed into the first MS via a syringe, and electrospray ionization (ESI) was conducted. ESI performs the dual action of discarding the solvent, and ionizing the lipids into precursor ions possessing a distinct mass to charge ratio (m/z). Sphingolipid subclasses display a unique molecular decomposition pattern [168, 169]; a pattern that is usefully exploited when conducting sensitive sphingolipid detection. Decomposition of the precursor ions was accomplished via the use of a collision cell in the second MS, which generates product ions that also possess a distinct m/z. Sphingolipids were subsequently detected by multiple reaction monitoring (MRM) based on m/z of both the precursor and product ions.

J. Statistical analysis

All data shown are averages of two independent experiments. Quantitative data are expressed as mean ± S.D. Student's t-test (two-tailed) was used for analysis of significance. $P<0.05$ was considered significant. Pearson's correlation coefficient was used to determine the linear relationship in a set of interdependent data.

CHAPTER IV
RESULTS

A. Rec700-Induced A549 Cell Death

To first identify the MOI (pfu/cell) to be used in downstream experiments, A549 cells were infected with various MOIs of *rec700* (wt virus), and cell death was measured by trypan dye exclusion at 48 hours post-infection (hpi) (Figure 8, A). The MOI of 40pfu/cell was selected for future experiments since it induced greater cell death (41%) compared to the MOI of 5pfu/cell (13%). Additionally, the MOI of 40pfu/cell ensured 100% adsorption of cultured cells as evidenced microscopically by their complete detachment at 48 hpi. The time-course of A549 cell death was then investigated at 40pfu/cell (Figure 8, B). Cell death began to increase significantly at around 36 hpi, reaching 39% and 68% at 48 and 72 hpi respectively, whereas mock-infected cells maintained their viability at all time-points.

B. *Rec700* Gene Expression in A549 Cells

To gain a thorough understanding of how *rec700* gene expression proceeds in A549 cells, viral *early* mRNA expression was monitored by RT-PCR during a 48 hour infection period. The E1A unit is transcribed shortly after viral DNA enters the nucleus [31]. Our results accordingly show that E1A 9S, 12S, and 13S mRNAs are present at 6 hpi (Figure 9), with 12S and 13S exhibiting the greatest expression. The 13S isoform encodes the 289R protein, which contains the CR3 region necessary for transactivation of other early viral genes. The mRNAs of viral early units E1B (Figure 10), E3 (Figure 12), and E4 (Figure 13)

were detected at 6 hpi. Unlike the other early viral genes, E2 mRNAs began to strongly increase after 6 hpi (Figure 11); an unsurprising observation, since the E2 promoter depends on E4*orf*6/7 proteins for complete transactivation [118, 119]. The adenoviral death protein (ADP) of the E3 unit was initially transcribed at very low amounts at early time points (6 and 12 hpi), but increased in expression by roughly 100-fold at later time points.

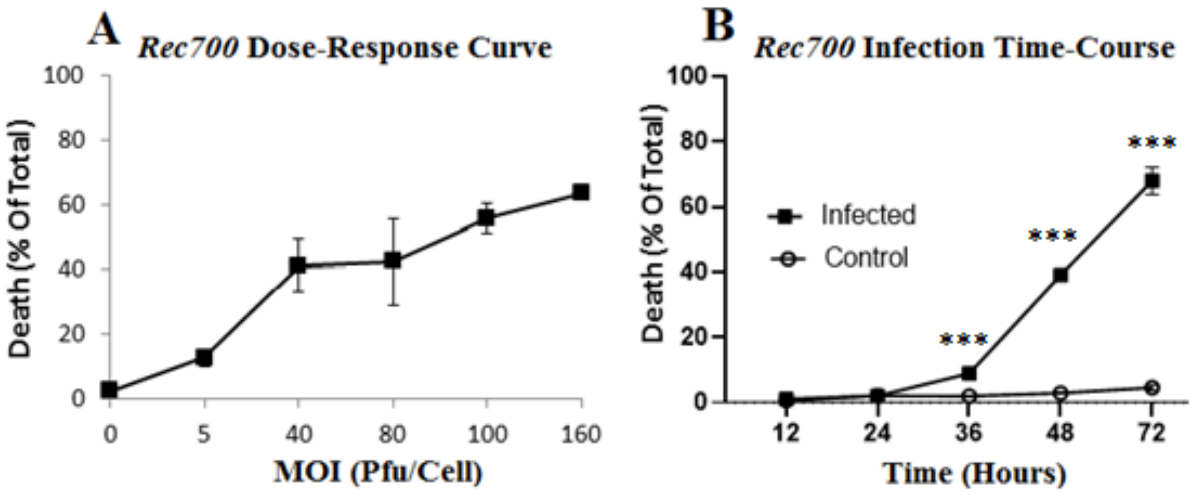

Figure 8: *E*ffect of *rec700* infection on A549 cell death. (A) A549 cells were infected with various MOIs of *rec700*, and cell death was measured at 48 hpi by trypan dye exclusion. Mock infected cells, not shown, exhibited <3% death. (B) A549 cells were infected at an MOI of 40pfu/cell, and cell death was measured by trypan dye exclusion between 12-72 hpi. Data is presented as mean ± S.D. ***P<0.001.

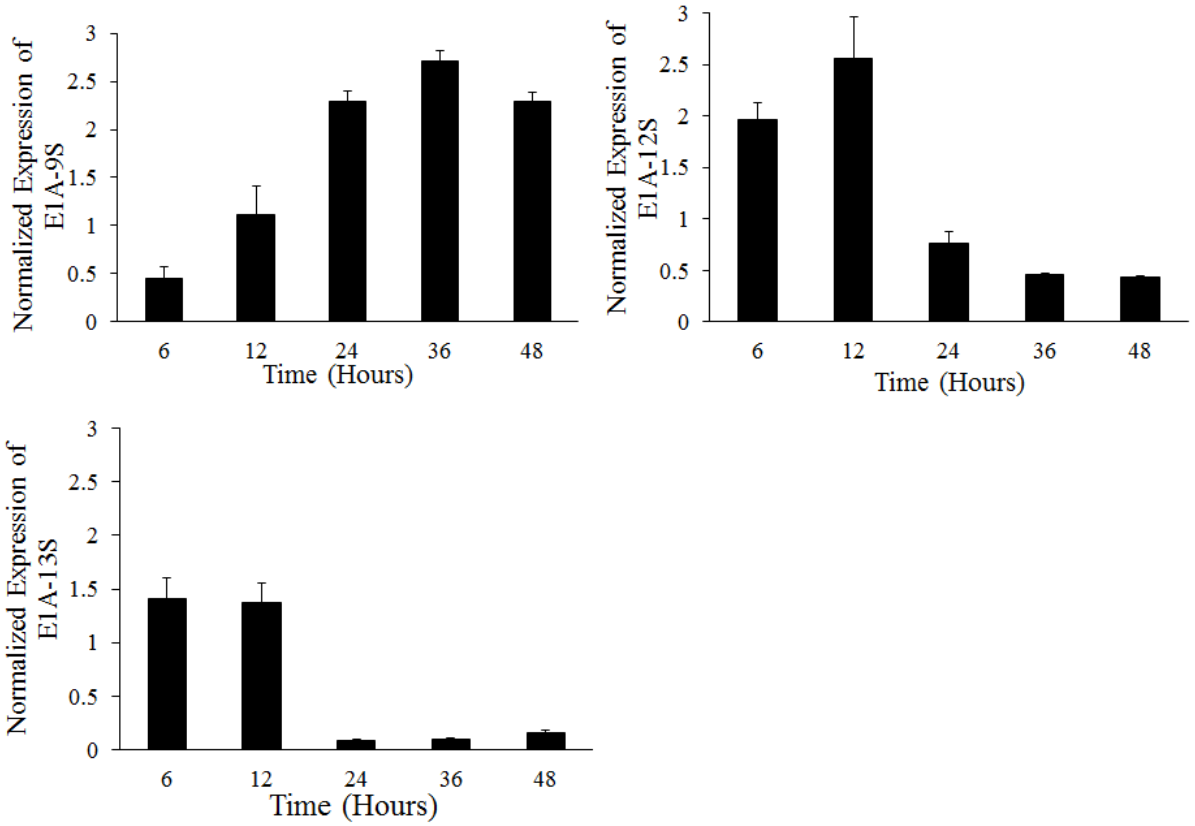

Figure 9: Relative gene expression of the E1A unit. A549 cells were infected with *rec700* at an MOI of 40pfu/cell and harvested at 6, 12, 24, 36, and 48 hpi. The mRNA expression level of the E1A unit was obtained by quantitative PCR and normalized with respect to GAPDH expression. Values are presented as mean ± S.D of two independent experiments.

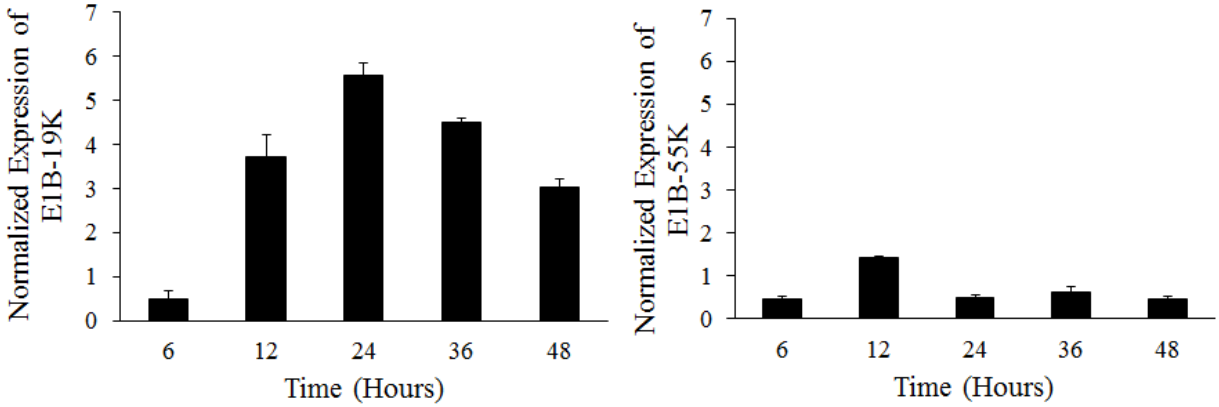

Figure 10: Relative gene expression of the E1B unit. A549 cells were infected with *rec700* at an MOI of 40pfu/cell and harvested at 6, 12, 24, 36, and 48 hpi. The mRNA expression level of the E1B unit was obtained by quantitative PCR and normalized with respect to GAPDH expression. Values are presented as mean ± S.D of two independent experiments.

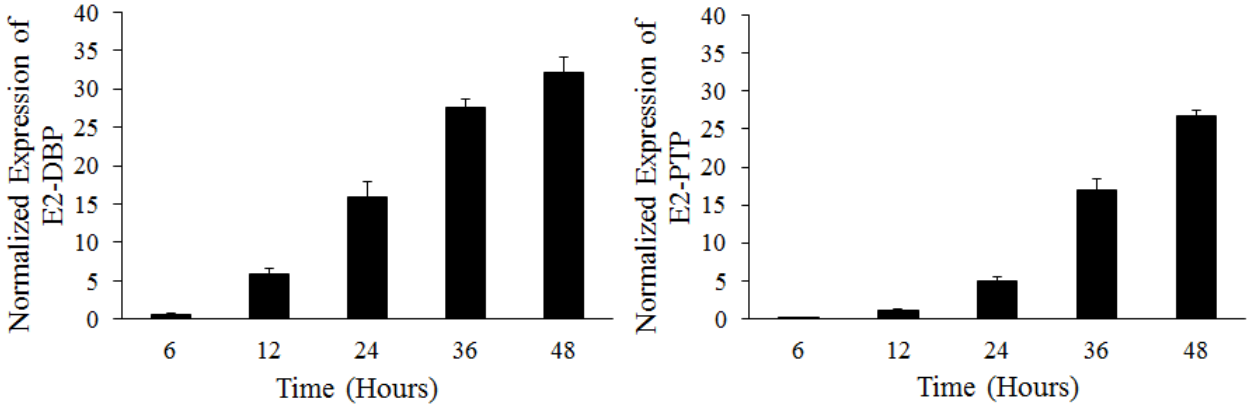

Figure 11: Relative gene expression of the E2A/E2B units. A549 cells were infected with *rec700* at an MOI of 40pfu/cell and harvested at 6, 12, 24, 36, and 48 hpi. The mRNA expression level of the E2A/E2B units were obtained by quantitative PCR and normalized with respect to GAPDH expression. Values are presented as mean ± S.D of two independent experiments.

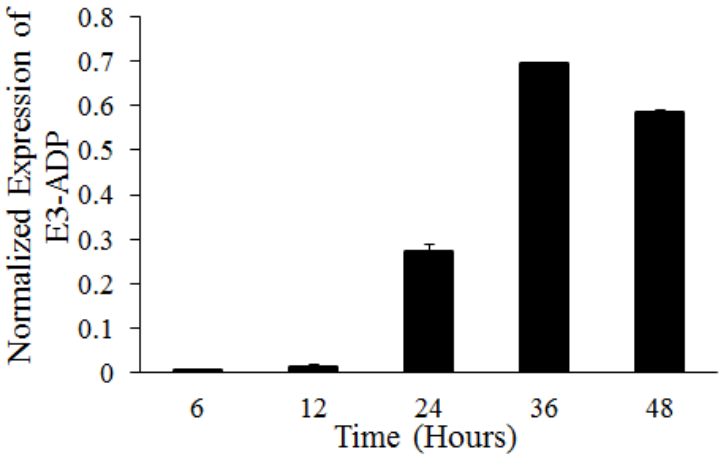

Figure 12: Relative gene expression of the E3-ADP. A549 cells were infected with *rec700* at an MOI of 40pfu/cell and harvested at 6, 12, 24, 36, and 48 hpi. The mRNA expression level of E3-ADP was obtained by quantitative PCR and normalized with respect to GAPDH expression. Values are presented as mean ± S.D of two independent experiments.

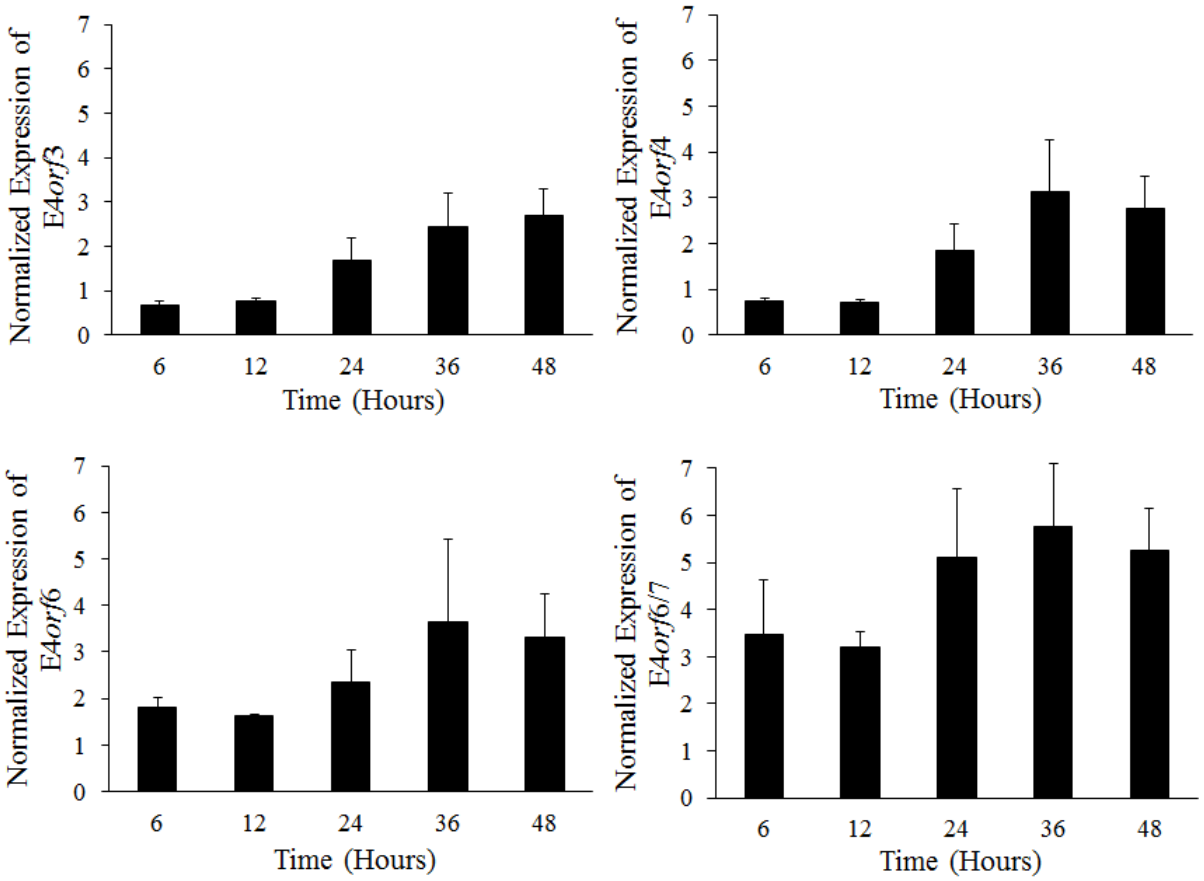

Figure 13: Relative gene expression of the E4 unit. A549 cells were infected with *rec700* at an MOI of 40pfu/cell and harvested at 6, 12, 24, 36, and 48 hpi. The mRNA expression level of the E4 unit bas obtained by quantitative PCR and normalized with respect to GAPDH expression. Values are presented as mean ± S.D of two independent experiments.

C. *Dl7001*-Induced A549 Cell Death

Dl7001, a *rec700* mutant that lacks the entire E3 unit, including ADP, was utilized for the purpose of detecting possible sphingolipid remodeling brought on by ADP. The time-course of *dl7001*-induced A549 cell death was investigated at an MOI equal to that used for *rec700* (40pfu/cell) and using the same viability assay (trypan dye exclusion). *Dl7001*-infected A549 cells began to exhibit significant cell death at around 72 hpi,

reaching 45% and 73% at 96 and 120 hpi respectively, whereas mock-infected cells maintained their viability at all time points (Figure 14). A significantly delayed cell lysis (~2 days) was brought on by *dl7001* when compared with *rec700*.

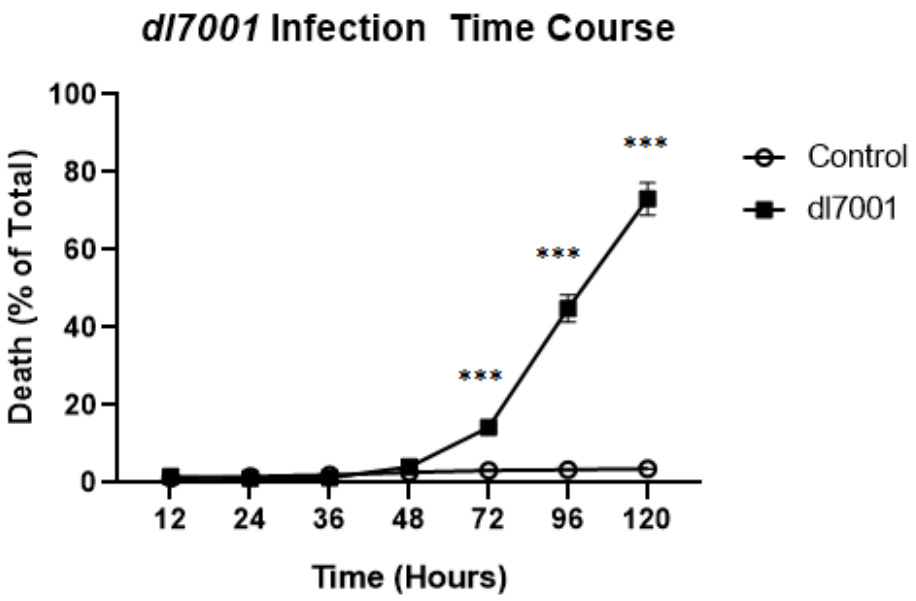

Figure 14: *E*ffect of *dl7001* infection on A549 cell death. A549 cells were infected at an MOI of 40pfu/cell, and cell death was measured by trypan dye exclusion between 12-120 hpi. Values are presented as mean ± SD of two independent experiments. ***P<0.001.

D. Sphingolipid Metabolism Gene Expression in *Rec700*-Infected A549 Cells

Gene expression analysis of some key sphingolipid metabolism enzymes was performed in *rec700*-infected A549 cells. Results show that *rec700* alters the gene expression of numerous enzymes of the sphingolipid metabolism pathway relative to

controls. The 2 subunits (SPT1 and SPT2) of the rate-limiting *de novo* pathway enzyme, SPT, were upregulated at early time-points, then subsequently downregulated at later time-points (Figure 15). KDSR and DEGS, which catalyze the second and fourth *de novo* pathway steps respectively, were downregulated to various degrees (Figures 16 and 18). On the other hand, the various ceramide synthase (CerS) isoforms appear to have been modified differently. CerS3 appears to have been upregulated, CerS4 downregulated, and Cer2/6 unaltered (Figure 17). Sphingosine kinase 1 (SK1) was significantly upregulated in *rec700*-infected cells (Figure 19). The enzyme which catalyzes the irreversible 'exit pathway' of sphingolipid metabolism, sphingosine-1-phosphate lyase (SPL), was gradually downregulated in *rec700*-infected cells (Figure 20). Neutral sphingomyelinase, which catalyzes sphingomyelin hydrolysis into ceramide, was gradually upregulated (Figure 21). These results show that *rec700* regulates the transcription of numerous sphingolipid metabolism enzymes, although only sphingosine kinase appears to have exhibited a significant alteration.

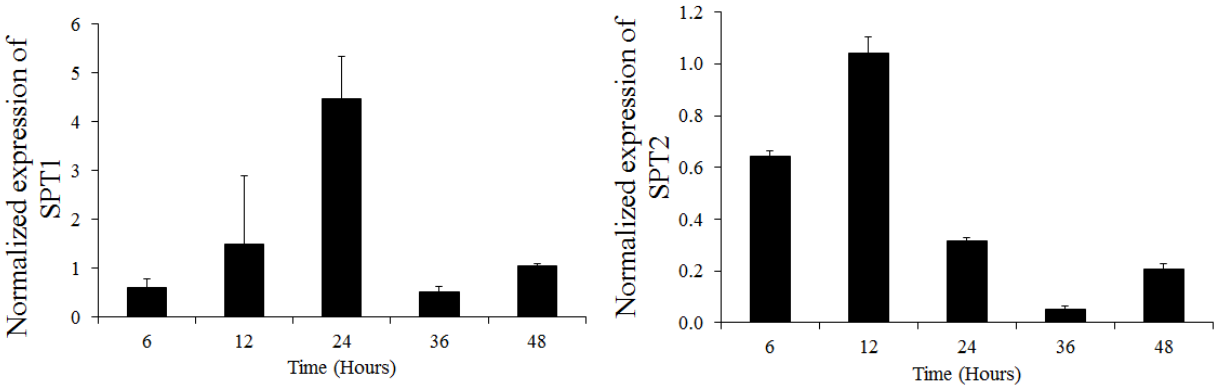

Figure 15: Relative gene expression of serine palmitoyltransferases (SPT1, SPT2). SPT mRNA was quantified via real-time PCR at 6, 12, 24, 36, and 48 hpi in *rec*700-infected A549 cells. Values are represented as delta-delta Ct, after normalizing to GAPDH and mock-infected controls.

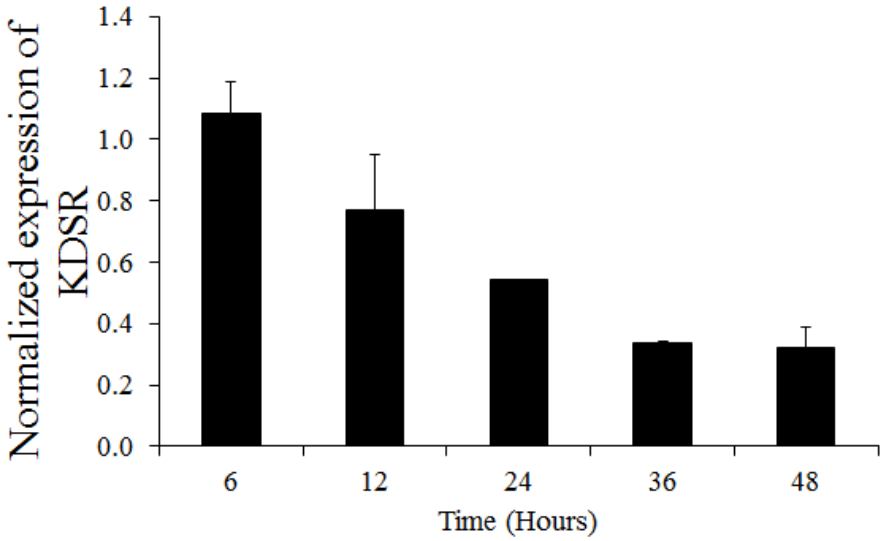

Figure 16: Relative gene expression of 3-ketodihydrosphingosine reductase (KDSR). KDSR mRNA was quantified via real-time PCR at 6, 12, 24, 36, and 48 hpi in *rec*700-infected A549 cells. Data is represented as delta-delta Ct, after normalizing to GAPDH and mock-infected controls.

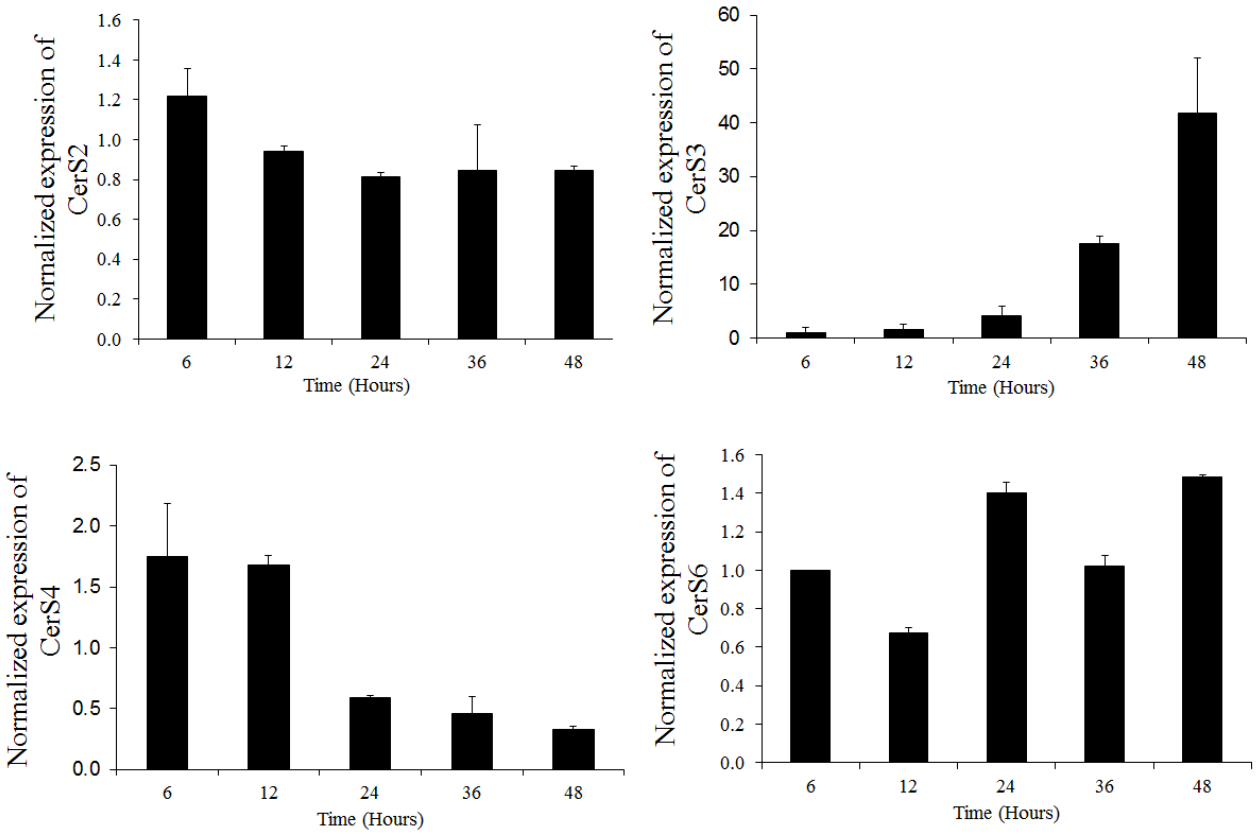

Figure 17: Normalized expression of ceramide synthases (CerS2, CerS3, CerS4, CerS6). CerS mRNA was quantified via real-time PCR at 6, 12, 24, 36, and 48 hpi in *rec*700-infected A549 cells. Data is represented as delta-delta Ct, after normalizing to GAPDH and mock-infected controls.

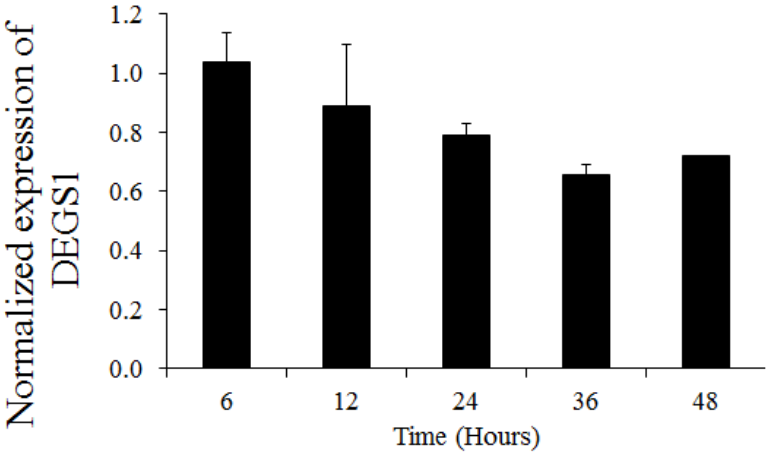

Figure 18: Normalized expression of dihydroceramide desaturase 1 (DEGS1). DEGS mRNA was quantified via real-time PCR at 6, 12, 24, 36, and 48 hpi in *rec*700-infected A549 cells. Data is represented as delta-delta Ct, after normalizing to GAPDH and mock-infected controls.

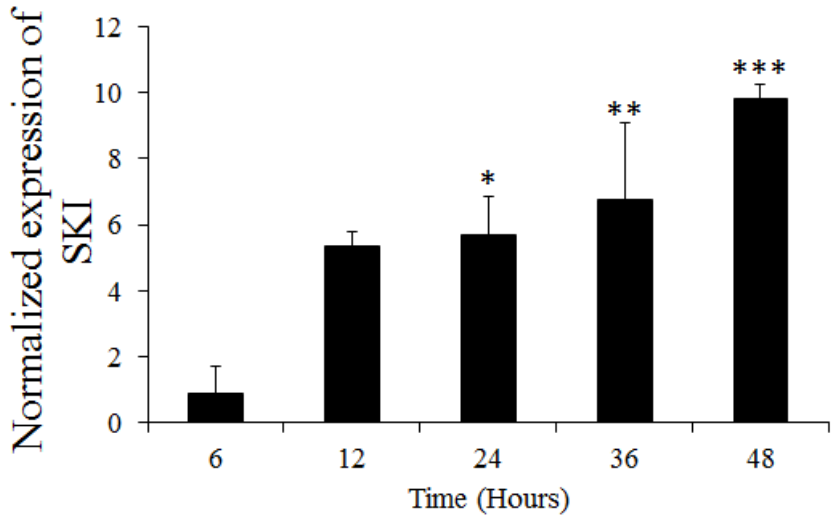

Figure 19: Normalized expression of sphingosine kinase 1 (SK1). SK mRNA was quantified via real-time PCR at 6, 12, 24, 36, and 48 hpi in *rec*700-infected A549 cells. Data is represented as delta-delta Ct, after normalizing to GAPDH and mock-infected controls. *P<0.05; **P<0.01; ***P<0.001

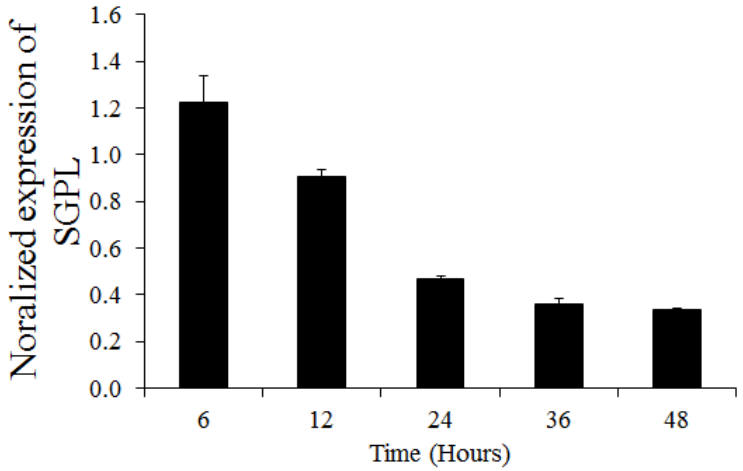

Figure 20: Normalized expression of sphingosine-1-phosphate lyase (SGPL). SGPL mRNA was quantified via real-time PCR at 6, 12, 24, 36, and 48 hpi in *rec*700-infected A549 cells. Data is represented as delta-delta Ct, after normalizing to GAPDH and mock-infected controls.

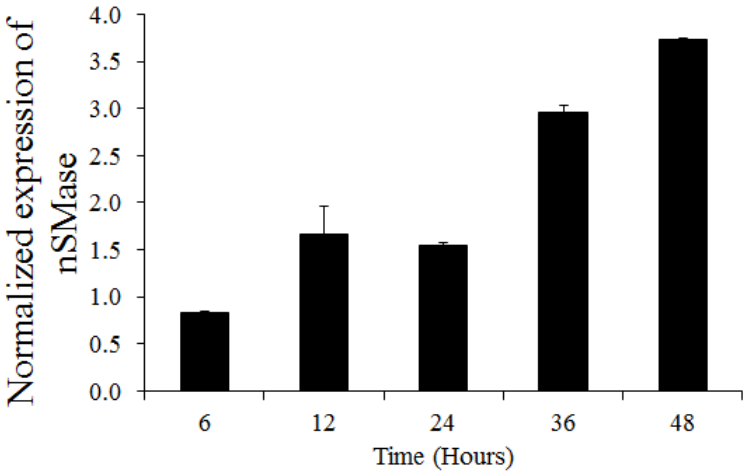

Figure 21: Normalized expression of neutral sphingomyelinase (nSMase). nSMase mRNA was quantified via real-time PCR at 6, 12, 24, 36, and 48 hpi in *rec*700-infected A549 cells. Data is represented as delta-delta Ct, after normalizing to GAPDH and mock-infected controls.

E. Sphingolipid Profile of A549 Cells

Since sphingolipids have emerged as effector molecules in cell death, the next step was to characterize the sphingolipidomic profile of *rec700*- and *dl7001*-infected A549 cells in order to identify any differential sphingolipid regulation between the two. Using LCMS, 86 sphingolipid species were quantified at various time-points (6, 12, 24, 36, and 48 hpi) in mock-infected A549 cells, in addition to A549 cells infected with either *rec700* or *dl7001* at an MOI of 40 pfu/cell. The 86 sphingolipid species include sphingosine, sphinganine, ceramides, dihydroceramides, sphingomyelins, dihydrosphingomyelins, gucosylceramides, dihydroglucosylceramides, lactosylceramides, and dihydrolactosylceramides. The sphingoid base of all the aforementioned species was of the C18 type, and the N-acyl chains (where applicable) ranged from C14 to C26 and were either saturated or monounsaturated.

An initial assessment of sphingolipids in mock-infected controls (6 hpi) indicates that sphingomyelins and dihydrosphingomyelins represent a significant majority (~94%) of the sphingolipids measured, with an almost equal proportion of sphingomyelins to dihydrosphingomyelins. Ceramides and glucosylceramides represented 4% and 1%, respectively, followed by a cohort of sphingolipids that were ≤1% in abundance (Figure 15, A;B). Identical results were obtained for *rec700* and *dl7001*-infected A549 cells harvested at 6 hpi, indicating that no significant sphingolipid remodeling took place at this time.

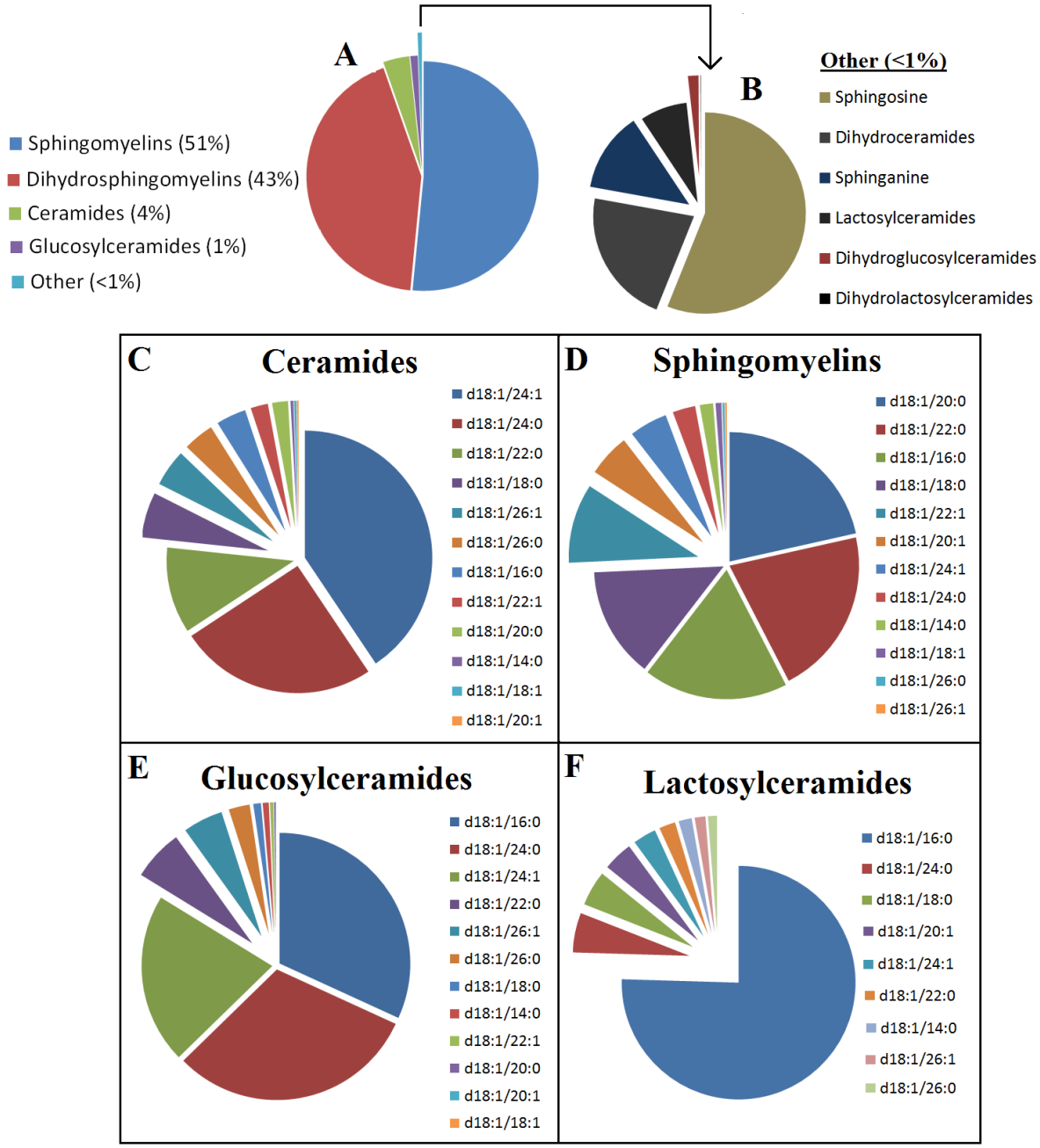

Figure 22: Sphingolipid profiling of A549 cells. LC-MS was used to assess the relative abundances of sphingolipid classes in non-infected A549 cells. We assessed the levels of sphinganine, sphingosine, (C) ceramides, (D), sphingomyelins, (E) glucosylceramides, and (F) lactosylceramides. Most dihydro-counterparts were negligible in amount (B), with the exception of dihydrosphingomyelins, which were almost identical in composition to sphingomyelins.

F. Sphinganine Levels Drop Significantly in *Rec700*-Infected A549 Cells

An initial assessment of sphinganine levels was performed, considering that this metabolite is typically generated in the *de novo* pathway. Results indicated that sphinganine levels significantly dropped at 24 hpi in *rec700*-infected cells relative to controls, with an even greater downregulation at later time-points (Figure 20, A). On the other hand, there was no significant alteration in sphinganine levels across the time-points in *dl7001*-infected cells relative to controls (Figure 20 ,B).

G. Opposite profiles of dihydroceramides and ceramides in *rec700*- versus *dl7001*-infected A549 cells

Dihydroceramides, which are generated from the precursor sphinganine in the *de novo* pathway via the action of ceramide synthases, were next assessed. Results indicate that total dihydroceramides significantly increased starting at 24 hpi in *rec700*-infected cells, with an even greater increase at later time-points (Figure 21, A). The individual species significantly upregulated were d18:0/14:0, d18:0/20:0, d18:0/22:0, d18:0/24:0, d18:0/24:1, and d18:0/26:0 (data not shown). On the other hand, *dl7001*-infected cells displayed no such elevation in total dihydroceramides (Figure 21, B), and the only species significantly upregulated was d18:0/24:0 (data not shown). The opposite was observed among ceramides, whereby total ceramides significantly accumulated starting at 24 hpi in *dl7001*-infected cells (figure 22 B), whereas no such accumulation was observed in *rec700*-infected cells (figure 22, A). In terms of individual ceramide species, d18:1/14:0, d18:1/16:0, d18:1/18:0, d18:1/24:0, and d18:1/26:0 were significantly upregulated in

dl7001-infected cell (data not shown), whereas d18:0/24:0 was the only species that was significantly upregulated in *rec700*-infected cells (data not shown).

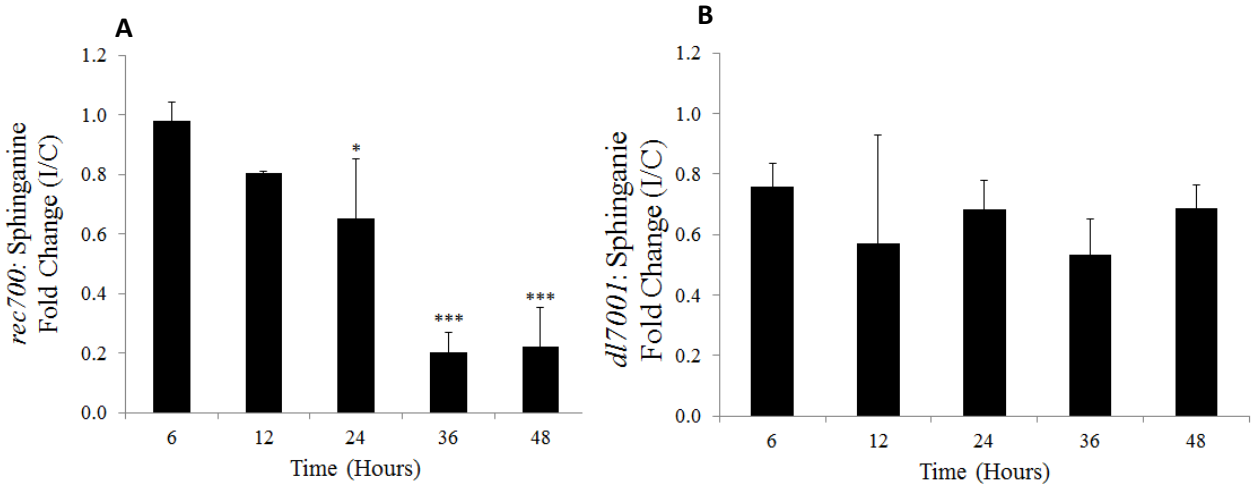

Figure 23: Sphinganine quantification. LCMS was used to quantify sphinganine, a metabolite of the *de novo* ceramide pathway, in both (A) *rec700*-infected and (B) *dl7001*-infected A549 cells. Data is presented as mean ± S.D of fold change (infected/controls). *P<0.05; ***P<0.001

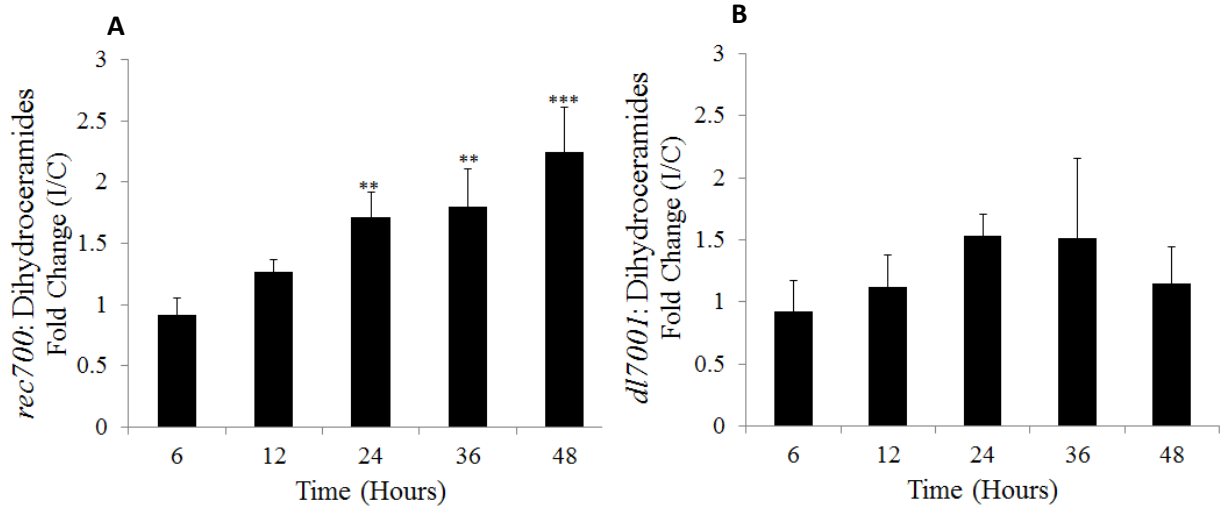

Figure 24: Dihydroceramide quantification. LCMS was used to quantify dihydroceramides, metabolites of the *de novo* ceramide pathway, in both (A) *rec700*-infected and (B) *dl7001*-infected A549 cells. Data is presented as mean ± S.D of fold change (infected/controls). **P<0.01; ***P<0.001.

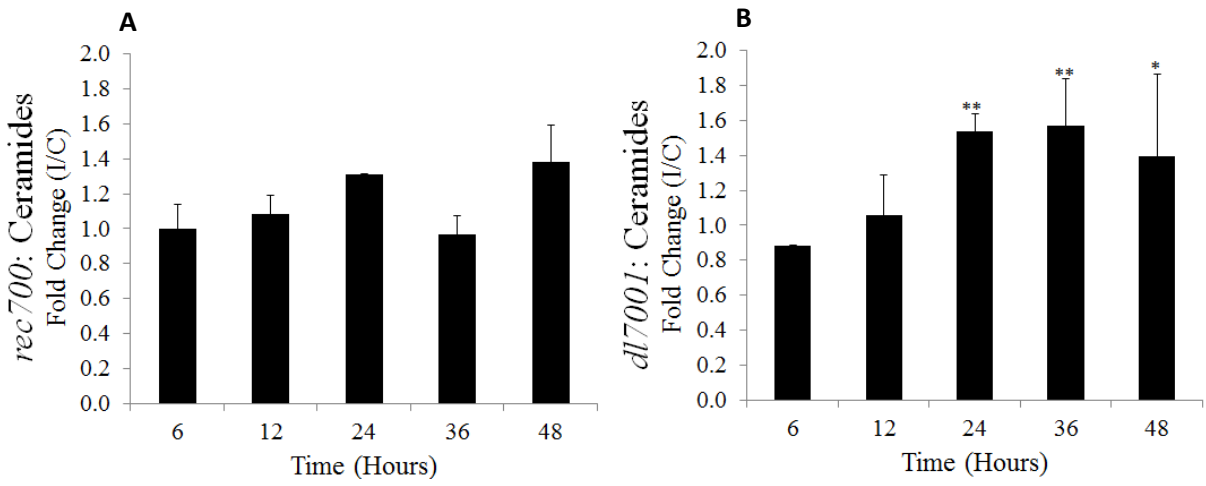

Figure 25: Ceramide quantification. LCMS was used to quantify dihydroceramides in both (A) *rec700*-infected and (B) *dl7001*-infected A549 cells. Data is presented as mean ± S.D of fold change (infected/controls). *P<0.05, **P<0.01

H. The E3 adenoviral Unit Does Not Downregulate the Protein Expression Levels of DEGS

The absence of a significant increase in ceramides in *rec700*-infected cell, despite the significant increase in dihydroceramides, led us to speculate that the E3 unit was negatively regulating DEGS activity. DEGS mRNA was not significantly downregulated (Figure 18), and we therefore performed a western blot analysis of the DEGS protein. Results indicate that there was no significant decrease in DEGS protein expression levels relative to controls, and levels alternatively appear to have increased at late time-points, albeit not significantly (Figure 26).

I. Significant alterations in sphingomyelins and glucosylceramides in *rec700*-infected A549 cells

Numerous sphingomyelin and dihydrosphingomyelin species were significantly decreased at 36 and 48 hpi in *rec700*-infected cells relative to controls (data not shown).

These species include d18:1/24:0, d18:1/26:0, d18:1/20:1, d18:0/20:0, and d18:0/26:1. Additionally, numerous glucosylceramide species were significantly elevated at late time-points in *rec700*-infected cells relative to controls (data not shown). These species include d18:1/16:0, d18:1/18:0, d18:1/22:0, and d18:1/24:1. In contrast, *dl7001*-infected cells exhibited no such alterations in sphingomyelins or glucosylceramides.

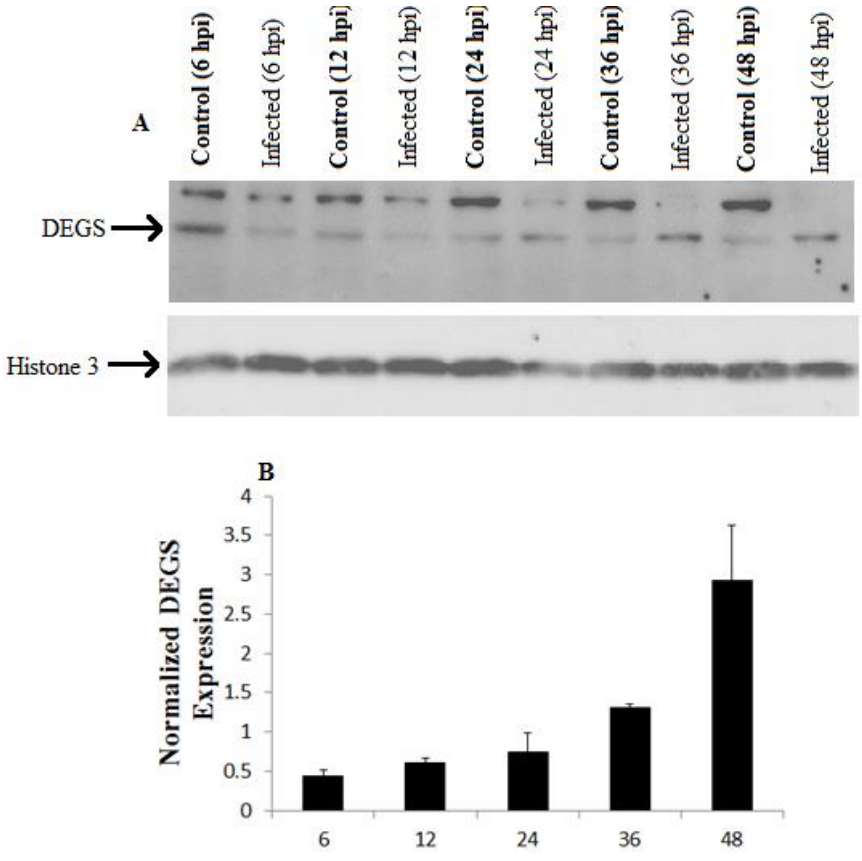

Figure 26: DEGS protein expression. A549 cells were infected with *rec700* at an MOI of 40 pfu/cell, and harvested at 6, 12, 24, 36, and 48 hpi. Protein expression levels of DEGS were assessed by western blotting, and Histone 3 was used as an internal house-keeping gene. A) DEGS (38 KDa) and Histone 3 (11 KDa) are shown. B) Band intensity was quantified using ImageJ software, and data is represented as mean ± S.D of fold change (infected/control) after normalizing for Histone 3.

J. Sphingosine Levels Drop Significantly in Both *Rec700*- and *Dl7001*-Infected A549 Cells

LC-MS data indicates that sphingosine levels dropped significantly in both *rec700*- (figure 27, A) and *dl7001*- (figure 27, B) infected A549 cells, although the former exhibited a sharper decrease.

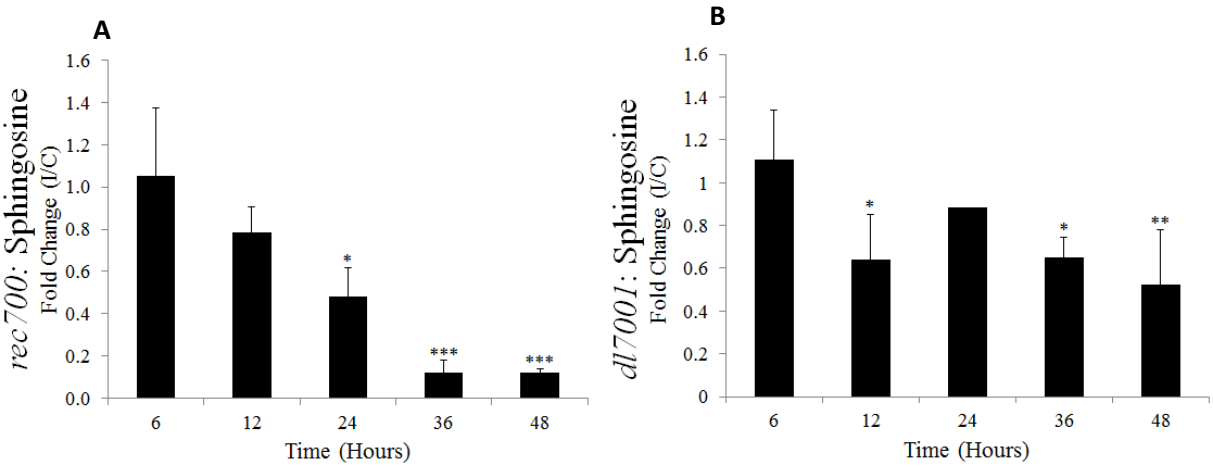

Figure 27: Sphingosine quantification. LCMS was used to quantify sphingosine in both (A) *rec700*-infected and (B) *dl7001*-infected A549 cells. Data is presented as mean ± S.D of fold change (infected/controls). *P<0.05; **P<0.01; ***P<0.001.

CHAPTER V

DISCUSSION

In this study, an LC-MS based sphingolipidomics approach was utilized in order to characterize the host cell's sphingolipid changes during HAdV infection. HAdVs are non-enveloped virions that typically infect epithelial cells and induce host cell lysis at the end of the infectious cycle, however this mechanism has not been fully elucidated. Sphingolipids are a large class of lipids that serve as membrane components [141] and regulators of cell growth, apoptosis, differentiation, migration, autophagy, and cell-cell/cell-matrix interactions [142, 143]. Ceramide is the central metabolite in the sphingolipid network, and it may be generated either via the *de novo* pathway, sphingomyelin hydrolysis, or alternatively via the salvage pathway.

Previous data showed that MCF-7 cells infected with either the wild-type HAdV *rec700* or the E3-deleted mutant *dl7001* accumulated considerable amounts of "ceramide" starting at 24 hpi. Such an accumulation was shown to occur in other viral types as well, such as influenza [170]. The purpose behind the use of *dl7001* was in order to observe any sphingolipid differences brought on by ADP, since this latter protein is the major driver for cell lysis post-infection. *Rec700*-infected cells began to lyse at 36 hpi, whereas *dl700l*-infected cells lacking the E3 unit (and notably ADP) unsurprisingly exhibited no significant cell death within the course of 48 hours [138]. This study suggested that the *de novo* pathway was implicated in cell lysis induction by HAdVs since accumulation of "ceramide" was identified to be mostly of *de novo* origin; the inhibition of the *de novo*

pathway using an SPT inhibitor myriocin, or the CerS inhibitor fumonisin, abrogated the accumulation [138]. The inhibition of the *de novo* pathway also resulted in a delayed cell death in *rec700*-infected cells. *dl7001*-infected cells also activate the *de novo* pathway, but lyse cells in a significantly delayed manner. It is important to note that in these earlier experiments, the diacylglycerol kinase (DGK) assay was used to measure ceramide levels. In this assay, both ceramide and dihydroceramide are phosphorylated by DGK in the presence of radioactive labeled ATP and their products are measured by scraping from thin layer chromatography (TLC). The resulting spots of ceramide phosphate and dihydroceramide phosphate are frequently indistinguishable as they overlap significantly. This limitation of the DGK assay used previously led to the inability to distinguish between ceramides and dihydroceramides. In the current work, we show that ceramide and dihydroceramide are differentially regulated by the two related viruses.

Our results showed that *dl7001* began to significantly induce cell lysis at 72 hpi, indicating a lag of roughly 1.5 days compared to *rec700*. *Rec700*-infected cells appear to exhibit cytoplasmic vacuolizations within the 48 hour duration; vacuolization is a common observation among virus-infected cells, and is usually an indication of their impending death [171, 172]. Additionally, *rec700*-and *dl7001* infected cells undergo a non-apoptotic cell death as evidenced by the lack of significant PARP cleavage [138]. The absence of PARP cleavage is likely due to the E1B-19K protein, a viral homologue of the anti-apoptotic cellular protein Bcl2 [47, 48].

Sphinganine is a metabolite generated in the *de novo* pathway, and its levels at any given time point depend on the relative actions of KDSR and CerS enzymes which regulate

its generation and depletion, respectively. This metabolite was significantly downregulated in *rec700*-infected cells relative to controls. Conversely, although there was a trend of diminished sphinganine levels in *dl7001*-infected cells, the result was not significant. KDSR gene expression was downregulated in *rec700*-infected cells, albeit not significantly. Similarly, the 4 CerS enzymes were differentially regulated whereby CerS3 and CerS4 expression increased and decreased, respectively. Although the *de novo* pathway is activated in both *rec700*- and *dl7001*-infected cells, there is no clear explanation as of yet that could account for the differences in sphinganine levels except depletion by increased activity, not expression, of downstream enzymes.

Perhaps the most striking result was the opposite dihydroceramide/ceramide profile observed in *rec700*- versus *dl7001*-infected cells. A significant increase in dihydrocramides was observed in *rec700*-infected cells starting at 24 hpi, with no significant increase in ceramides. In contrast, *dl7001*-infected cells displayed a significant increase in ceramides starting at 36 hpi, with no significant increase in dihydroceramides. Since it is established that ceramides are generated mostly via the *de novo* pathway in HAdV-infected cells, these results implicate the DEGS enzyme, which converts dihydroceramides into ceramides in the final step of the *de novo* pathway. This finding leads us to suggest that an E3 protein is involved in the negative regulation of DEGS function, considering that ceramides were significantly upregulated in cells infected with *dl7001* which lacks the E3 unit. Since no significant downregulation of DEGS gene or protein expression was observed in *rec700*-infected cells, it is likely that DEGS may have been negatively regulated post-transcriptionally. DEGS protein levels were not significantly downregulated either, and

instead appear to have increased at late time points. Although DEGS protein levels appear to have remained constant, and perhaps increased, this is no indication of the activity of DEGS, which may be regulated via several mechanisms [173-175]. Gene expression analysis of CerS isoforms in *rec700*-infected cells indicates that CerS3 was upregulated, which coincides with the upregulation observed in several dihydroceramide species in *rec700*-infected cells (d18:0/22:0, d18:0/22:0, d18:0/24:0, d18:0/24:1). Although CerS4 was downregulated, it typically incorporates acyl chain lengths of 18 and 20 carbons, similar to CerS3. Therefore, it appears that CerS3 upregulation counteracted the downregulation of CerS4.

The sphingomyelinase pathway was actually not activated in *rec700*-infected cells, despite the significant decrease of most sphingomyelin and dihydrosphingomyelin species at 36 and 48 hpi. Several points of evidence led to this conclusion: Firstly, sphingomyelins/dihydrosphingomyelins are considerably greater in abundance than ceramides/dihydroceramides [176], and our LC/MS results indicate accordingly that sphingomyelins/dihydrosphingomyleins (~21,500 pmol/mg) are ~2500% more abundant than ceramides/dihydroceramides (~870 pmol/mg). Therefore, even minor reductions in the former would significantly elevate the latter; an effect that was not observed, as total ceramides were not significantly elevated. Secondly, a previous study showed that the *de novo* pathway was mostly responsible for 'ceramide' accumulation in *rec700*-infected A549 cells [138]. Thirdly, our results show that *rec700*-infected A549 cells began to undergo significant cell lysis at 36 hpi, as measured by trypan dye inclusion which detects plasma membrane permeabilization. Significant sphingomyelin and dihydrosphingomyelin

decreases began at this time-point as well, and it is likely that these species, which typically localize at the non-cytosolic (luminal) side of the plasma membranes, were being shed from the membrane and were subsequently disposed of within the debris. In confirmation of this latter hypothesis, *dl7001*-infected A549 cells, which begin to lyse starting at 72 hpi, did not exhibit any significant decreases in sphingomyelin/dihydrosphingomyelin during the time-points measured.

Rec700-induced glucosylceramide elevation may be explained either via the action of glucosylceramide synthase, or alternatively via the breakdown of lactosylceramide into glucosylceramide. LCMS data indicates that lactosylceramides were negligible in amounts relative to glucosylceramides, and additionally were not significantly downregulated (data not shown). The likely candidate behind the increase in glucosylceramide is therefore the conversion of ceramide into glucosylceramide via the action of glucosylceramide synthase. Interestingly, the glycosylation of ceramide via glucosylceramide synthase (UGCG) has been identified as a mechanism by which cancer cells maintain their progression [177-180]. Therefore, the significant upregulation of glucosylceramides by adenoviral-infected cells may serve as a cellular attempt at survival.

The significant decrease in sphingosine observed during both *rec700* and *dl7001* infections may be explained either via the 'salvaging' of sphingosine into ceramide, or alternatively the conversion of sphingosine into S1P via the action of sphingosine kinase. LC-MS was unable to detect S1P in our model, despite the favorable method of lipid extraction used. This is likely due to the sub-picomole expression levels of S1P, and hence an evaded detection. This hypothesis is confirmed by the fact that LC-MS was able to

detect S1P levels in other studies from our lab involving influenza virus infection of A549 cells, which utilized the same lipid extraction methodology. The significant upregulation of sphingosine kinase mRNA in *rec700*-infected cells did not coincide with increased S1P, and this may be explained either via the inhibited translation of sphingosine kinase mRNA, or alternatively via the post-translation modification of sphingosine kinase. Very interestingly, an increase in cytoplasmic calcium causes calcium and integrin-binding protein 1 (CIBP1) to transport SK1 to the plasma membrane [181], which subsequently leads to the enhanced secretion of S1P from cells [181, 182]. This possibly explains why S1P was not detected, as the paracrine function of S1P would render it undetectable during cellular lipid extraction. In line with this hypothesis, ADP has been proposed to function as a 'viroporin' [183], a membrane-bound oligomer that promotes the diffusion of calcium into the cytoplasm. It is likely, therefore, that ADP promoted the excretion of S1P. mRNA expression of ADP indicates that it greatly increases in expression at 24 hpi, which coincides with the time at which sphingosine kinase significantly increases. Sphingosine may have partially been converted into ceramide via the salvage pathway. Sphingosine is typically a membrane bound metabolite, and is mostly present in the ER due to the latter's massive membranous composition. Ceramide synthases, which are present in the ER, are able to generate ceramides directly from sphingosine. However, no significant accumulation of ceramide was observed in *rec700*-infected A549 cells. This is due to the relatively small amounts of sphingosine (~100pmol/mg) in comparison to total ceramides (~1000pmol/mg), and considering that a portion of ceramides were subsequently converted to glucosylceramides.

Numerous studies have implicated dihydroceramides in the induction of autophagy [156-158] and the induction of an autophagic type of cell death [159, 184]. Autophagy during adenoviral infection has indeed been identified [185-188]. Importantly, autophagy correlated with cell lysis during adenoviral infection [188]. However, whether the significant generation of dihydroceramides observed during *rec700* infection serves as the initiator of autophagy is not demonstrably clear at this point. This matter will be addressed in future studies.

CHAPTER VI

CONCLUSION

In this study, we have shown that the E3 unit of HAdVs is implicated in inducing sphingolipid alterations, namely the stark dihydroceramide/ceramide difference observed across *rec700*- and *dl7001*-infected cells. DEGS did not undergo any significant downregulation at the mRNA or the protein levels, and we speculate that enzymatic activity is negatively regulated. Whether the inhibition of DEGS and the subsequent accumulation of dihydroceramide in *rec700*-infected cells serves a role in HAdV-induced cell lysis is not clear at this point, and further studies will be conducted to elucidate the role of spingolipids in HAdV-induced cell lysis.

CHAPTER VII

FUTURE PERSPECTIVES

Numerous experiments will be performed to investigate the activities of sphingolipid enzymes during adenoviral infection, such as DEGS. A sphingomyelinase assay will be performed to rule out the involvement of sphingomyelin hydrolysis in *rec700*-infected cells. Further experiments will be conducted on cells infected with *rec700*- and several adenoviral mutants in order to draw the mechanism by which sphingolipid alterations impact cell lysis. In our present study, it is unknown which of the seven E3 proteins (6.7K, 10.4K, 11.6K, 12.5K, 14.5K, 14.7K, or 19K) induced the sphingolipid alterations that distinguished *rec700*- versus *dl7001*-infected A549 cells. Our use of available E3 mutants dl799 (¯/₋ 10.4K and 14.5K), dl798 (¯/₋ 14.5K), dl748 (¯/₋ all except 14.5K), and dl309 (¯/₋ 10.4K, 14.5K, and 14.7K) would allow us to implicate 10.4K, 14.5K, or 14.7K. Additionally, we will acquire dl712, a mutant that produces all proteins except ADP, which would allow us to identify whether ADP is implicated in the differential results obtained across *rec700* and *dl7001*. Finally, LC-MS will be applied on cells infected with two *rec700* mutants, dl1011 (¯/₋ E4 unit) and dl1014 (¯/₋ E4 unit, except E4*orf*4), in order to discern any sphingolipidomic alterations brought on by E4*orf*4.

REFERENCES

1. Rowe, W.P., et al., *Isolation of a cytopathogenic agent from human adenoids undergoing spontaneous degeneration in tissue culture.* Proc Soc Exp Biol Med, 1953. **84**(3): p. 570-3.
2. Davison, A.J., M. Benko, and B. Harrach, *Genetic content and evolution of adenoviruses.* J Gen Virol, 2003. **84**(Pt 11): p. 2895-908.
3. Lynch, J.P., 3rd, M. Fishbein, and M. Echavarria, *Adenovirus.* Semin Respir Crit Care Med, 2011. **32**(4): p. 494-511.
4. Saitoh-Inagawa, W., et al., *Ten years' surveillance of viral conjunctivitis in Sapporo, Japan.* Graefes Arch Clin Exp Ophthalmol, 1999. **237**(1): p. 35-8.
5. Grimwood, K., et al., *Patients with enteric adenovirus gastroenteritis admitted to an Australian pediatric teaching hospital from 1981 to 1992.* J Clin Microbiol, 1995. **33**(1): p. 131-6.
6. Crawford-Miksza, L.K., R.N. Nang, and D.P. Schnurr, *Strain variation in adenovirus serotypes 4 and 7a causing acute respiratory disease.* J Clin Microbiol, 1999. **37**(4): p. 1107-12.
7. Dudding, B.A., et al., *Fatal pneumonia associated with adenovirus type 7 in three military trainees.* N Engl J Med, 1972. **286**(24): p. 1289-92.
8. Atkinson, R.L., *Viruses as an etiology of obesity.* Mayo Clin Proc, 2007. **82**(10): p. 1192-8.
9. Hierholzer, J.C., *Adenoviruses in the immunocompromised host.* Clin Microbiol Rev, 1992. **5**(3): p. 262-74.
10. Crenshaw, B.J., et al., *Perspective on Adenoviruses: Epidemiology, Pathogenicity, and Gene Therapy.* Biomedicines, 2019. **7**(3).
11. Khanal, S., P. Ghimire, and A.S. Dhamoon, *The Repertoire of Adenovirus in Human Disease: The Innocuous to the Deadly.* Biomedicines, 2018. **6**(1).
12. Wold, W.S. and K. Toth, *Adenovirus vectors for gene therapy, vaccination and cancer gene therapy.* Curr Gene Ther, 2013. **13**(6): p. 421-33.
13. Alemany, R., C. Balague, and D.T. Curiel, *Replicative adenoviruses for cancer therapy.* Nat Biotechnol, 2000. **18**(7): p. 723-7.
14. Kirn, D., *Replication-selective oncolytic adenoviruses: virotherapy aimed at genetic targets in cancer.* Oncogene, 2000. **19**(56): p. 6660-9.
15. Fabry, C.M., et al., *A quasi-atomic model of human adenovirus type 5 capsid.* EMBO J, 2005. **24**(9): p. 1645-54.
16. Chatterjee, P.K., M.E. Vayda, and S.J. Flint, *Identification of proteins and protein domains that contact DNA within adenovirus nucleoprotein cores by ultraviolet light crosslinking of oligonucleotides 32P-labelled in vivo.* J Mol Biol, 1986. **188**(1): p. 23-37.
17. van Oostrum, J. and R.M. Burnett, *Molecular composition of the adenovirus type 2 virion.* J Virol, 1985. **56**(2): p. 439-48.
18. Lehmberg, E., et al., *Reversed-phase high-performance liquid chromatographic assay for the adenovirus type 5 proteome.* J Chromatogr B Biomed Sci Appl, 1999. **732**(2): p. 411-23.
19. Giberson, A.N., A.R. Davidson, and R.J. Parks, *Chromatin structure of adenovirus DNA throughout infection.* Nucleic Acids Res, 2012. **40**(6): p. 2369-76.
20. Bergelson, J.M., et al., *Isolation of a common receptor for Coxsackie B viruses and adenoviruses 2 and 5.* Science, 1997. **275**(5304): p. 1320-3.

21. Coyne, C.B. and J.M. Bergelson, *CAR: a virus receptor within the tight junction.* Adv Drug Deliv Rev, 2005. **57**(6): p. 869-82.
22. Wickham, T.J., et al., *Integrins alpha v beta 3 and alpha v beta 5 promote adenovirus internalization but not virus attachment.* Cell, 1993. **73**(2): p. 309-19.
23. Meier, O. and U.F. Greber, *Adenovirus endocytosis.* J Gene Med, 2004. **6 Suppl 1**: p. S152-63.
24. Greber, U.F., et al., *The role of the adenovirus protease on virus entry into cells.* EMBO J, 1996. **15**(8): p. 1766-77.
25. Greber, U.F., et al., *Stepwise dismantling of adenovirus 2 during entry into cells.* Cell, 1993. **75**(3): p. 477-86.
26. Wodrich, H., et al., *A capsid-encoded PPxY-motif facilitates adenovirus entry.* PLoS Pathog, 2010. **6**(3): p. e1000808.
27. Trotman, L.C., et al., *Import of adenovirus DNA involves the nuclear pore complex receptor CAN/Nup214 and histone H1.* Nat Cell Biol, 2001. **3**(12): p. 1092-100.
28. Mishoe, H., et al., *In vitro transcription initiation by purified RNA polymerase II within the adenovirus 2 major late promoter region.* J Biol Chem, 1984. **259**(4): p. 2236-42.
29. Kidd, A.H., D. Garwicz, and M. Oberg, *Human and simian adenoviruses: phylogenetic inferences from analysis of VA RNA genes.* Virology, 1995. **207**(1): p. 32-45.
30. Fessler, S.P. and C.S. Young, *Control of adenovirus early gene expression during the late phase of infection.* J Virol, 1998. **72**(5): p. 4049-56.
31. King, C.R., et al., *Hacking the Cell: Network Intrusion and Exploitation by Adenovirus E1A.* MBio, 2018. **9**(3).
32. Moran, E., et al., *Identification of separate domains in the adenovirus E1A gene for immortalization activity and the activation of virus early genes.* Mol Cell Biol, 1986. **6**(10): p. 3470-80.
33. Moran, E. and M.B. Mathews, *Multiple functional domains in the adenovirus E1A gene.* Cell, 1987. **48**(2): p. 177-8.
34. Arroyo, M. and P. Raychaudhuri, *Retinoblastoma-repression of E2F-dependent transcription depends on the ability of the retinoblastoma protein to interact with E2F and is abrogated by the adenovirus E1A oncoprotein.* Nucleic Acids Res, 1992. **20**(22): p. 5947-54.
35. Mittnacht, S., et al., *Distinct sub-populations of the retinoblastoma protein show a distinct pattern of phosphorylation.* EMBO J, 1994. **13**(1): p. 118-27.
36. Trimarchi, J.M. and J.A. Lees, *Sibling rivalry in the E2F family.* Nat Rev Mol Cell Biol, 2002. **3**(1): p. 11-20.
37. Deleu, L., et al., *Recruitment of TRRAP required for oncogenic transformation by E1A.* Oncogene, 2001. **20**(57): p. 8270-5.
38. Chinnadurai, G., *Modulation of oncogenic transformation by the human adenovirus E1A C-terminal region.* Curr Top Microbiol Immunol, 2004. **273**: p. 139-61.
39. Arany, Z., et al., *A family of transcriptional adaptor proteins targeted by the E1A oncoprotein.* Nature, 1995. **374**(6517): p. 81-4.
40. Bannister, A.J. and T. Kouzarides, *The CBP co-activator is a histone acetyltransferase.* Nature, 1996. **384**(6610): p. 641-3.
41. Berk, A.J. and P.A. Sharp, *Structure of the adenovirus 2 early mRNAs.* Cell, 1978. **14**(3): p. 695-711.

42. Spector, D.J., M. McGrogan, and H.J. Raskas, *Regulation of the appearance of cytoplasmic RNAs from region 1 of the adenovirus 2 genome.* J Mol Biol, 1978. **126**(3): p. 395-414.
43. Babich, A. and J.R. Nevins, *The stability of early adenovirus mRNA is controlled by the viral 72 kd DNA-binding protein.* Cell, 1981. **26**(3 Pt 1): p. 371-9.
44. Mymryk, J.S., K. Shire, and S.T. Bayley, *Induction of apoptosis by adenovirus type 5 E1A in rat cells requires a proliferation block.* Oncogene, 1994. **9**(4): p. 1187-93.
45. Querido, E., J.G. Teodoro, and P.E. Branton, *Accumulation of p53 induced by the adenovirus E1A protein requires regions involved in the stimulation of DNA synthesis.* J Virol, 1997. **71**(5): p. 3526-33.
46. Duerksen-Hughes, P., W.S. Wold, and L.R. Gooding, *Adenovirus E1A renders infected cells sensitive to cytolysis by tumor necrosis factor.* J Immunol, 1989. **143**(12): p. 4193-200.
47. Farrow, S.N., et al., *Cloning of a bcl-2 homologue by interaction with adenovirus E1B 19K.* Nature, 1995. **374**(6524): p. 731-3.
48. Han, J., et al., *The E1B 19K protein blocks apoptosis by interacting with and inhibiting the p53-inducible and death-promoting Bax protein.* Genes Dev, 1996. **10**(4): p. 461-77.
49. Hardwick, J.M. and L. Soane, *Multiple functions of BCL-2 family proteins.* Cold Spring Harb Perspect Biol, 2013. **5**(2).
50. Yew, P.R. and A.J. Berk, *Inhibition of p53 transactivation required for transformation by adenovirus early 1B protein.* Nature, 1992. **357**(6373): p. 82-5.
51. Gonzalez, R., et al., *Adenovirus E1B 55-kilodalton protein is required for both regulation of mRNA export and efficient entry into the late phase of infection in normal human fibroblasts.* J Virol, 2006. **80**(2): p. 964-74.
52. Babich, A., et al., *Effect of adenovirus on metabolism of specific host mRNAs: transport control and specific translational discrimination.* Mol Cell Biol, 1983. **3**(7): p. 1212-21.
53. Chow, L.T., T.R. Broker, and J.B. Lewis, *Complex splicing patterns of RNAs from the early regions of adenovirus-2.* J Mol Biol, 1979. **134**(2): p. 265-303.
54. Stillman, B.W., et al., *Identification of the gene and mRNA for the adenovirus terminal protein precursor.* Cell, 1981. **23**(2): p. 497-508.
55. Brenkman, A.B., E.C. Breure, and P.C. van der Vliet, *Molecular architecture of adenovirus DNA polymerase and location of the protein primer.* J Virol, 2002. **76**(16): p. 8200-7.
56. King, A.J., W.R. Teertstra, and P.C. van der Vliet, *Dissociation of the protein primer and DNA polymerase after initiation of adenovirus DNA replication.* J Biol Chem, 1997. **272**(39): p. 24617-23.
57. Liu, H., J.H. Naismith, and R.T. Hay, *Adenovirus DNA replication.* Curr Top Microbiol Immunol, 2003. **272**: p. 131-64.
58. Nagata, K., et al., *Adenovirus DNA replication in vitro: identification of a host factor that stimulates synthesis of the preterminal protein-dCMP complex.* Proc Natl Acad Sci U S A, 1982. **79**(21): p. 6438-42.
59. Nicolas, J.C., et al., *Host range temperature-conditional mutants in the adenovirus DNA binding protein are defective in the assembly of infectious virus.* Virology, 1983. **126**(1): p. 228-39.
60. Toth, K., et al., *Adenovirus immunoregulatory E3 proteins prolong transplants of human cells in immunocompetent mice.* Virus Res, 2005. **108**(1-2): p. 149-59.
61. Morin, J.E., et al., *Recombinant adenovirus induces antibody response to hepatitis B virus surface antigen in hamsters.* Proc Natl Acad Sci U S A, 1987. **84**(13): p. 4626-30.

62. Cladaras, C. and W.S. Wold, *DNA sequence of the early E3 transcription unit of adenovirus 5.* Virology, 1985. **140**(1): p. 28-43.
63. Wilson-Rawls, J., et al., *A 6700 MW membrane protein is encoded by region E3 of adenovirus type 2.* Virology, 1990. **178**(1): p. 204-12.
64. Tollefson, A.E., et al., *A 10,400-molecular-weight membrane protein is coded by region E3 of adenovirus.* J Virol, 1990. **64**(2): p. 794-801.
65. Wold, W.S., et al., *Mapping a new gene that encodes an 11,600-molecular-weight protein in the E3 transcription unit of adenovirus 2.* J Virol, 1984. **52**(2): p. 307-13.
66. Hawkins, L.K. and W.S. Wold, *A 12,500 MW protein is coded by region E3 of adenovirus.* Virology, 1992. **188**(2): p. 486-94.
67. Tollefson, A.E., et al., *A 14,500 MW protein is coded by region E3 of group C human adenoviruses.* Virology, 1990. **175**(1): p. 19-29.
68. Tollefson, A.E. and W.S. Wold, *Identification and gene mapping of a 14,700-molecular-weight protein encoded by region E3 of group C adenoviruses.* J Virol, 1988. **62**(1): p. 33-9.
69. Persson, H., M. Jansson, and L. Philipson, *Synthesis and genomic site for an adenovirus type 2 early glycoprotein.* J Mol Biol, 1980. **136**(4): p. 375-94.
70. Wilson-Rawls, J. and W.S. Wold, *The E3-6.7K protein of adenovirus is an Asn-linked integral membrane glycoprotein localized in the endoplasmic reticulum.* Virology, 1993. **195**(1): p. 6-15.
71. Benedict, C.A., et al., *Three adenovirus E3 proteins cooperate to evade apoptosis by tumor necrosis factor-related apoptosis-inducing ligand receptor-1 and -2.* J Biol Chem, 2001. **276**(5): p. 3270-8.
72. Moise, A.R., et al., *Adenovirus E3-6.7K maintains calcium homeostasis and prevents apoptosis and arachidonic acid release.* J Virol, 2002. **76**(4): p. 1578-87.
73. Tollefson, A.E., et al., *The 10,400- and 14,500-dalton proteins encoded by region E3 of adenovirus form a complex and function together to down-regulate the epidermal growth factor receptor.* J Virol, 1991. **65**(6): p. 3095-105.
74. Stewart, A.R., et al., *The adenovirus E3 10.4K and 14.5K proteins, which function to prevent cytolysis by tumor necrosis factor and to down-regulate the epidermal growth factor receptor, are localized in the plasma membrane.* J Virol, 1995. **69**(1): p. 172-81.
75. Tollefson, A.E., et al., *Forced degradation of Fas inhibits apoptosis in adenovirus-infected cells.* Nature, 1998. **392**(6677): p. 726-30.
76. Elsing, A. and H.G. Burgert, *The adenovirus E3/10.4K-14.5K proteins down-modulate the apoptosis receptor Fas/Apo-1 by inducing its internalization.* Proc Natl Acad Sci U S A, 1998. **95**(17): p. 10072-7.
77. Tollefson, A.E., et al., *Inhibition of TRAIL-induced apoptosis and forced internalization of TRAIL receptor 1 by adenovirus proteins.* J Virol, 2001. **75**(19): p. 8875-87.
78. Friedman, J.M. and M.S. Horwitz, *Inhibition of tumor necrosis factor alpha-induced NF-kappa B activation by the adenovirus E3-10.4/14.5K complex.* J Virol, 2002. **76**(11): p. 5515-21.
79. Carlin, C.R., et al., *Epidermal growth factor receptor is down-regulated by a 10,400 MW protein encoded by the E3 region of adenovirus.* Cell, 1989. **57**(1): p. 135-44.
80. Scaria, A., et al., *The E3-11.6K protein of adenovirus is an Asn-glycosylated integral membrane protein that localizes to the nuclear membrane.* Virology, 1992. **191**(2): p. 743-53.

81. Tollefson, A.E., et al., *The 11,600-MW protein encoded by region E3 of adenovirus is expressed early but is greatly amplified at late stages of infection.* J Virol, 1992. **66**(6): p. 3633-42.
82. Tollefson, A.E., et al., *The adenovirus death protein (E3-11.6K) is required at very late stages of infection for efficient cell lysis and release of adenovirus from infected cells.* J Virol, 1996. **70**(4): p. 2296-306.
83. Ying, B. and W.S. Wold, *Adenovirus ADP protein (E3-11.6K), which is required for efficient cell lysis and virus release, interacts with human MAD2B.* Virology, 2003. **313**(1): p. 224-34.
84. Gooding, L.R., et al., *The adenovirus E3-14.7K protein is a general inhibitor of tumor necrosis factor-mediated cytolysis.* J Immunol, 1990. **145**(9): p. 3080-6.
85. Li, Y., J. Kang, and M.S. Horwitz, *Interaction of an adenovirus E3 14.7-kilodalton protein with a novel tumor necrosis factor alpha-inducible cellular protein containing leucine zipper domains.* Mol Cell Biol, 1998. **18**(3): p. 1601-10.
86. Gooding, L.R., et al., *A 14,700 MW protein from the E3 region of adenovirus inhibits cytolysis by tumor necrosis factor.* Cell, 1988. **53**(3): p. 341-6.
87. Krajcsi, P., et al., *The adenovirus E3-14.7K protein and the E3-10.4K/14.5K complex of proteins, which independently inhibit tumor necrosis factor (TNF)-induced apoptosis, also independently inhibit TNF-induced release of arachidonic acid.* J Virol, 1996. **70**(8): p. 4904-13.
88. Thorne, T.E., et al., *The activity of cytosolic phospholipase A2 is required for the lysis of adenovirus-infected cells by tumor necrosis factor.* J Virol, 1996. **70**(12): p. 8502-7.
89. Li, Y., et al., *Identification of a cell protein (FIP-3) as a modulator of NF-kappaB activity and as a target of an adenovirus inhibitor of tumor necrosis factor alpha-induced apoptosis.* Proc Natl Acad Sci U S A, 1999. **96**(3): p. 1042-7.
90. Li, Y., J. Kang, and M.S. Horwitz, *Interaction of an adenovirus 14.7-kilodalton protein inhibitor of tumor necrosis factor alpha cytolysis with a new member of the GTPase superfamily of signal transducers.* J Virol, 1997. **71**(2): p. 1576-82.
91. Lukashok, S.A., et al., *An adenovirus inhibitor of tumor necrosis factor alpha-induced apoptosis complexes with dynein and a small GTPase.* J Virol, 2000. **74**(10): p. 4705-9.
92. Mercurio, F., et al., *IkappaB kinase (IKK)-associated protein 1, a common component of the heterogeneous IKK complex.* Mol Cell Biol, 1999. **19**(2): p. 1526-38.
93. Rothwarf, D.M., et al., *IKK-gamma is an essential regulatory subunit of the IkappaB kinase complex.* Nature, 1998. **395**(6699): p. 297-300.
94. Yamaoka, S., et al., *Complementation cloning of NEMO, a component of the IkappaB kinase complex essential for NF-kappaB activation.* Cell, 1998. **93**(7): p. 1231-40.
95. Paabo, S., et al., *A short sequence in the COOH-terminus makes an adenovirus membrane glycoprotein a resident of the endoplasmic reticulum.* Cell, 1987. **50**(2): p. 311-7.
96. Bennett, E.M., et al., *Cutting edge: adenovirus E19 has two mechanisms for affecting class I MHC expression.* J Immunol, 1999. **162**(9): p. 5049-52.
97. McSharry, B.P., et al., *Adenovirus E3/19K promotes evasion of NK cell recognition by intracellular sequestration of the NKG2D ligands major histocompatibility complex class I chain-related proteins A and B.* J Virol, 2008. **82**(9): p. 4585-94.
98. Virtanen, A., et al., *mRNAs from human adenovirus 2 early region 4.* J Virol, 1984. **51**(3): p. 822-31.
99. Tigges, M.A. and H.J. Raskas, *Splice junctions in adenovirus 2 early region 4 mRNAs: multiple splice sites produce 18 to 24 RNAs.* J Virol, 1984. **50**(1): p. 106-17.

100. Thai, M., et al., *Adenovirus E4ORF1-induced MYC activation promotes host cell anabolic glucose metabolism and virus replication.* Cell Metab, 2014. **19**(4): p. 694-701.
101. Sarnow, P., et al., *Identification and characterization of an immunologically conserved adenovirus early region 11,000 Mr protein and its association with the nuclear matrix.* J Mol Biol, 1982. **162**(3): p. 565-83.
102. Carvalho, T., et al., *Targeting of adenovirus E1A and E4-ORF3 proteins to nuclear matrix-associated PML bodies.* J Cell Biol, 1995. **131**(1): p. 45-56.
103. Borden, K.L., *Pondering the promyelocytic leukemia protein (PML) puzzle: possible functions for PML nuclear bodies.* Mol Cell Biol, 2002. **22**(15): p. 5259-69.
104. Stracker, T.H., et al., *Serotype-specific reorganization of the Mre11 complex by adenoviral E4orf3 proteins.* J Virol, 2005. **79**(11): p. 6664-73.
105. Sohn, S.Y. and P. Hearing, *The adenovirus E4-ORF3 protein functions as a SUMO E3 ligase for TIF-1gamma sumoylation and poly-SUMO chain elongation.* Proc Natl Acad Sci U S A, 2016. **113**(24): p. 6725-30.
106. Kleinberger, T. and T. Shenk, *Adenovirus E4orf4 protein binds to protein phosphatase 2A, and the complex down regulates E1A-enhanced junB transcription.* J Virol, 1993. **67**(12): p. 7556-60.
107. Champagne, C., et al., *Activation of adenovirus type 2 early region 4 ORF4 cytoplasmic death function by direct binding to Src kinase domain.* J Biol Chem, 2004. **279**(24): p. 25905-15.
108. Kanopka, A., et al., *Regulation of adenovirus alternative RNA splicing by dephosphorylation of SR proteins.* Nature, 1998. **393**(6681): p. 185-7.
109. Estmer Nilsson, C., et al., *The adenovirus E4-ORF4 splicing enhancer protein interacts with a subset of phosphorylated SR proteins.* EMBO J, 2001. **20**(4): p. 864-71.
110. O'Shea, C., et al., *Adenoviral proteins mimic nutrient/growth signals to activate the mTOR pathway for viral replication.* EMBO J, 2005. **24**(6): p. 1211-21.
111. Lane, H.A., et al., *p70s6k function is essential for G1 progression.* Nature, 1993. **363**(6425): p. 170-2.
112. Dobner, T., et al., *Blockage by adenovirus E4orf6 of transcriptional activation by the p53 tumor suppressor.* Science, 1996. **272**(5267): p. 1470-3.
113. Sarnow, P., et al., *Adenovirus early region 1B 58,000-dalton tumor antigen is physically associated with an early region 4 25,000-dalton protein in productively infected cells.* J Virol, 1984. **49**(3): p. 692-700.
114. Huang, M.M. and P. Hearing, *Adenovirus early region 4 encodes two gene products with redundant effects in lytic infection.* J Virol, 1989. **63**(6): p. 2605-15.
115. Bridge, E. and G. Ketner, *Interaction of adenoviral E4 and E1b products in late gene expression.* Virology, 1990. **174**(2): p. 345-53.
116. Blanchette, P., et al., *Both BC-box motifs of adenovirus protein E4orf6 are required to efficiently assemble an E3 ligase complex that degrades p53.* Mol Cell Biol, 2004. **24**(21): p. 9619-29.
117. Harada, J.N., et al., *Analysis of the adenovirus E1B-55K-anchored proteome reveals its link to ubiquitination machinery.* J Virol, 2002. **76**(18): p. 9194-206.
118. Huang, M.M. and P. Hearing, *The adenovirus early region 4 open reading frame 6/7 protein regulates the DNA binding activity of the cellular transcription factor, E2F, through a direct complex.* Genes Dev, 1989. **3**(11): p. 1699-710.

119. Hardy, S., D.A. Engel, and T. Shenk, *An adenovirus early region 4 gene product is required for induction of the infection-specific form of cellular E2F activity.* Genes Dev, 1989. **3**(7): p. 1062-74.
120. Lutz, P., M. Rosa-Calatrava, and C. Kedinger, *The product of the adenovirus intermediate gene IX is a transcriptional activator.* J Virol, 1997. **71**(7): p. 5102-9.
121. Morris, S.J., G.E. Scott, and K.N. Leppard, *Adenovirus late-phase infection is controlled by a novel L4 promoter.* J Virol, 2010. **84**(14): p. 7096-104.
122. Shaw, A.R. and E.B. Ziff, *Transcripts from the adenovirus-2 major late promoter yield a single early family of 3' coterminal mRNAs and five late families.* Cell, 1980. **22**(3): p. 905-16.
123. Hasson, T.B., et al., *Adenovirus L1 52- and 55-kilodalton proteins are required for assembly of virions.* J Virol, 1989. **63**(9): p. 3612-21.
124. Gustin, K.E. and M.J. Imperiale, *Encapsidation of viral DNA requires the adenovirus L1 52/55-kilodalton protein.* J Virol, 1998. **72**(10): p. 7860-70.
125. Akusjarvi, G. and H. Persson, *Gene and mRNA for precursor polypeptide VI from adenovirus type 2.* J Virol, 1981. **38**(2): p. 469-82.
126. Le Moullec, J.M., et al., *Polyadenylic acid addition sites in the adenovirus type 2 major late transcription unit.* J Virol, 1983. **48**(1): p. 127-34.
127. Karen, K.A. and P. Hearing, *Adenovirus core protein VII protects the viral genome from a DNA damage response at early times after infection.* J Virol, 2011. **85**(9): p. 4135-42.
128. Prescott, J. and E. Falck-Pedersen, *Sequence elements upstream of the 3' cleavage site confer substrate strength to the adenovirus L1 and L3 polyadenylation sites.* Mol Cell Biol, 1994. **14**(7): p. 4682-93.
129. Weber, J.M., *Adenovirus endopeptidase and its role in virus infection.* Curr Top Microbiol Immunol, 1995. **199 (Pt 1)**: p. 227-35.
130. Sittler, A., H. Gallinaro, and M. Jacob, *Upstream and downstream cis-acting elements for cleavage at the L4 polyadenylation site of adenovirus-2.* Nucleic Acids Res, 1994. **22**(2): p. 222-31.
131. Wright, J. and K.N. Leppard, *The human adenovirus 5 L4 promoter is activated by cellular stress response protein p53.* J Virol, 2013. **87**(21): p. 11617-25.
132. Morris, S.J. and K.N. Leppard, *Adenovirus serotype 5 L4-22K and L4-33K proteins have distinct functions in regulating late gene expression.* J Virol, 2009. **83**(7): p. 3049-58.
133. Ostapchuk, P., et al., *The L4 22-kilodalton protein plays a role in packaging of the adenovirus genome.* J Virol, 2006. **80**(14): p. 6973-81.
134. Ahi, Y.S., S.V. Vemula, and S.K. Mittal, *Adenoviral E2 IVa2 protein interacts with L4 33K protein and E2 DNA-binding protein.* J Gen Virol, 2013. **94**(Pt 6): p. 1325-34.
135. Xi, Q., R. Cuesta, and R.J. Schneider, *Tethering of eIF4G to adenoviral mRNAs by viral 100k protein drives ribosome shunting.* Genes Dev, 2004. **18**(16): p. 1997-2009.
136. Murali, V.K., et al., *Adenovirus death protein (ADP) is required for lytic infection of human lymphocytes.* J Virol, 2014. **88**(2): p. 903-12.
137. Tollefson, A.E., et al., *The E3-11.6-kDa adenovirus death protein (ADP) is required for efficient cell death: characterization of cells infected with adp mutants.* Virology, 1996. **220**(1): p. 152-62.
138. Kanj, S.S., et al., *Ceramide regulates SR protein phosphorylation during adenoviral infection.* Virology, 2006. **345**(1): p. 280-9.

139. Yetukuri, L., et al., *Informatics and computational strategies for the study of lipids.* Mol Biosyst, 2008. **4**(2): p. 121-7.
140. Fahy, E., et al., *A comprehensive classification system for lipids.* J Lipid Res, 2005. **46**(5): p. 839-61.
141. Breslow, D.K. and J.S. Weissman, *Membranes in balance: mechanisms of sphingolipid homeostasis.* Mol Cell, 2010. **40**(2): p. 267-79.
142. Hannun, Y.A. and L.M. Obeid, *Principles of bioactive lipid signalling: lessons from sphingolipids.* Nat Rev Mol Cell Biol, 2008. **9**(2): p. 139-50.
143. Futerman, A.H. and Y.A. Hannun, *The complex life of simple sphingolipids.* EMBO Rep, 2004. **5**(8): p. 777-82.
144. Hojjati, M.R., Z. Li, and X.C. Jiang, *Serine palmitoyl-CoA transferase (SPT) deficiency and sphingolipid levels in mice.* Biochim Biophys Acta, 2005. **1737**(1): p. 44-51.
145. Mullen, T.D., Y.A. Hannun, and L.M. Obeid, *Ceramide synthases at the centre of sphingolipid metabolism and biology.* Biochem J, 2012. **441**(3): p. 789-802.
146. Levy, M. and A.H. Futerman, *Mammalian ceramide synthases.* IUBMB Life, 2010. **62**(5): p. 347-56.
147. Schulze, H., C. Michel, and G. van Echten-Deckert, *Dihydroceramide desaturase.* Methods Enzymol, 2000. **311**: p. 22-30.
148. Hanada, K., et al., *Molecular machinery for non-vesicular trafficking of ceramide.* Nature, 2003. **426**(6968): p. 803-9.
149. Gault, C.R., L.M. Obeid, and Y.A. Hannun, *An overview of sphingolipid metabolism: from synthesis to breakdown.* Adv Exp Med Biol, 2010. **688**: p. 1-23.
150. Morad, S.A. and M.C. Cabot, *Ceramide-orchestrated signalling in cancer cells.* Nat Rev Cancer, 2013. **13**(1): p. 51-65.
151. Kitatani, K., J. Idkowiak-Baldys, and Y.A. Hannun, *The sphingolipid salvage pathway in ceramide metabolism and signaling.* Cell Signal, 2008. **20**(6): p. 1010-8.
152. Cuvillier, O., et al., *[Sphingolipid-mediated apoptotic signaling pathways].* J Soc Biol, 2003. **197**(3): p. 217-21.
153. Maceyka, M., et al., *Sphingosine kinase, sphingosine-1-phosphate, and apoptosis.* Biochim Biophys Acta, 2002. **1585**(2-3): p. 193-201.
154. Bielawska, A., et al., *Selectivity of ceramide-mediated biology. Lack of activity of erythro-dihydroceramide.* J Biol Chem, 1993. **268**(35): p. 26226-32.
155. Ravid, T., et al., *Ceramide accumulation precedes caspase-3 activation during apoptosis of A549 human lung adenocarcinoma cells.* Am J Physiol Lung Cell Mol Physiol, 2003. **284**(6): p. L1082-92.
156. Zheng, W., et al., *Ceramides and other bioactive sphingolipid backbones in health and disease: lipidomic analysis, metabolism and roles in membrane structure, dynamics, signaling and autophagy.* Biochim Biophys Acta, 2006. **1758**(12): p. 1864-84.
157. Signorelli, P., et al., *Dihydroceramide intracellular increase in response to resveratrol treatment mediates autophagy in gastric cancer cells.* Cancer Lett, 2009. **282**(2): p. 238-43.
158. Gagliostro, V., et al., *Dihydroceramide delays cell cycle G1/S transition via activation of ER stress and induction of autophagy.* Int J Biochem Cell Biol, 2012. **44**(12): p. 2135-43.
159. Hernandez-Tiedra, S., et al., *Dihydroceramide accumulation mediates cytotoxic autophagy of cancer cells via autolysosome destabilization.* Autophagy, 2016. **12**(11): p. 2213-2229.
160. Jain, A., et al., *Diverting CERT-mediated ceramide transport to mitochondria triggers Bax-dependent apoptosis.* J Cell Sci, 2017. **130**(2): p. 360-371.

161. Siskind, L.J., et al., *The BCL-2 protein BAK is required for long-chain ceramide generation during apoptosis.* J Biol Chem, 2010. **285**(16): p. 11818-26.
162. Wold, W.S., et al., *Evidence that AGUAUAUGA and CCAAGAUGA initiate translation in the same mRNA region E3 of adenovirus.* Virology, 1986. **148**(1): p. 168-80.
163. Ranheim, T.S., et al., *Characterization of mutants within the gene for the adenovirus E3 14.7-kilodalton protein which prevents cytolysis by tumor necrosis factor.* J Virol, 1993. **67**(4): p. 2159-67.
164. Green, M. and W.S. Wold, *Human adenoviruses: growth, purification, and transfection assay.* Methods Enzymol, 1979. **58**: p. 425-35.
165. Lowry, O.H., et al., *Protein measurement with the Folin phenol reagent.* J Biol Chem, 1951. **193**(1): p. 265-75.
166. Radko, S., et al., *Effects of Adenovirus Type 5 E1A Isoforms on Viral Replication in Arrested Human Cells.* PLoS One, 2015. **10**(10): p. e0140124.
167. Bielawski, J., et al., *Comprehensive quantitative analysis of bioactive sphingolipids by high-performance liquid chromatography-tandem mass spectrometry.* Methods Mol Biol, 2009. **579**: p. 443-67.
168. Gu, M., et al., *Ceramide profiling of complex lipid mixtures by electrospray ionization mass spectrometry.* Anal Biochem, 1997. **244**(2): p. 347-56.
169. Sullards, M.C. and A.H. Merrill, Jr., *Analysis of sphingosine 1-phosphate, ceramides, and other bioactive sphingolipids by high-performance liquid chromatography-tandem mass spectrometry.* Sci STKE, 2001. **2001**(67): p. pl1.
170. Soudani, N., et al., *Ceramide Suppresses Influenza A Virus Replication In Vitro.* J Virol, 2019. **93**(7).
171. Henics, T. and D.N. Wheatley, *Cytoplasmic vacuolation, adaptation and cell death: a view on new perspectives and features.* Biol Cell, 1999. **91**(7): p. 485-98.
172. Tamm, I., *Cell injury with viruses.* Am J Pathol, 1975. **81**(1): p. 163-78.
173. Geeraert, L., G.P. Mannaerts, and P.P. van Veldhoven, *Conversion of dihydroceramide into ceramide: involvement of a desaturase.* Biochem J, 1997. **327 (Pt 1)**: p. 125-32.
174. Michel, C., et al., *Characterization of ceramide synthesis. A dihydroceramide desaturase introduces the 4,5-trans-double bond of sphingosine at the level of dihydroceramide.* J Biol Chem, 1997. **272**(36): p. 22432-7.
175. Idkowiak-Baldys, J., et al., *Dihydroceramide desaturase activity is modulated by oxidative stress.* Biochem J, 2010. **427**(2): p. 265-74.
176. Bielawski, J., et al., *Simultaneous quantitative analysis of bioactive sphingolipids by high-performance liquid chromatography-tandem mass spectrometry.* Methods, 2006. **39**(2): p. 82-91.
177. Hakomori, S.I., *Glycosynaptic microdomains controlling tumor cell phenotype through alteration of cell growth, adhesion, and motility.* FEBS Lett, 2010. **584**(9): p. 1901-6.
178. Liu, Y.Y., et al., *Ceramide glycosylation potentiates cellular multidrug resistance.* FASEB J, 2001. **15**(3): p. 719-30.
179. Ogretmen, B. and Y.A. Hannun, *Biologically active sphingolipids in cancer pathogenesis and treatment.* Nat Rev Cancer, 2004. **4**(8): p. 604-16.
180. Patwardhan, G.A. and Y.Y. Liu, *Sphingolipids and expression regulation of genes in cancer.* Prog Lipid Res, 2011. **50**(1): p. 104-14.
181. Jarman, K.E., et al., *Translocation of sphingosine kinase 1 to the plasma membrane is mediated by calcium- and integrin-binding protein 1.* J Biol Chem, 2010. **285**(1): p. 483-92.

182. Pitson, S.M., et al., *Activation of sphingosine kinase 1 by ERK1/2-mediated phosphorylation.* EMBO J, 2003. **22**(20): p. 5491-500.
183. Carrasco, L., *Modification of membrane permeability by animal viruses.* Adv Virus Res, 1995. **45**: p. 61-112.
184. Levine, B., *Cell biology: autophagy and cancer.* Nature, 2007. **446**(7137): p. 745-7.
185. Ito, H., et al., *Autophagic cell death of malignant glioma cells induced by a conditionally replicating adenovirus.* J Natl Cancer Inst, 2006. **98**(9): p. 625-36.
186. Jiang, H., et al., *Examination of the therapeutic potential of Delta-24-RGD in brain tumor stem cells: role of autophagic cell death.* J Natl Cancer Inst, 2007. **99**(18): p. 1410-4.
187. Baehrecke, E.H., *Autophagy: dual roles in life and death?* Nat Rev Mol Cell Biol, 2005. **6**(6): p. 505-10.
188. Jiang, H., et al., *Human adenovirus type 5 induces cell lysis through autophagy and autophagy-triggered caspase activity.* J Virol, 2011. **85**(10): p. 4720-9.